EPJ Web of Conferences **22**, 00007 (2012)
DOI: 10.1051/epjconf/20122200007

Extensions and some recent applications of the Landau theory of phase transitions

P. Tolédano

Laboratoire de Physique des Systèmes Complexes, Université de Picardie, 33 rue Saint-Leu, 80000 Amiens, France

The basic concepts of the Landau theory of phase transitions are introduced through working examples. A number of rules governing the application of the theory to second and first-order transitions are given. The approach to magnetostructural transitions in magnetic mulltiferroic materials is detailed. Examples of transitions induced by replica of the same order-parameter in superconducting and liquid crystal systems, are described. The theory of reconstructive transitions is outlined and illustrated by the examples of the graphite-diamond transition and by the phase diagram of iron. An extention of the phenomenological approach to incommensurate structures to the crystal-amorphous transition is proposed (see also the chapter by Perez-Mato *et al*. for further discussion and applications).

1. INTRODUCTION

In the pioneering article of Landau [1] the phenomenological theory of phase transitions intended to establish the mutual compatibility of the symmetry and physical characteristics of a phase transition: Relationship between the symmetry of the phases, consistency between the nature of the symmetry change and the nature of the physical quantities behaving anomalously across the transition. This aim was achieved by means of introducing the concepts of *order-parameter* and *Landau free-energy*. Although in its initial formulation the theory considered the simple case of continuous (second-order) transitions induced by a single irreducible representation between group-subgroup related phases, it proved subsequently to apply, providing suitable extensions, to discontinuous (first-order) transitions [2], to transitions associated with several order-parameters [2], or to reconstructive transitions involving a loss of the group-subgroup relationship [3]. The theory was used to describe almost all types of phase transitions occurring in hard or soft condensed matter physics, such as structural and magnetic transitions in crystalline materials [4], the superconducting [5] and superfluid [6] transitions, the liquid-solid [7] and liquid-vapour [8] transitions, and the variety of transitions disclosed in liquid crystals [9] and complex fluids [10]. After introducing the basic concepts of the Landau theory (Sec. 2) and some rules governing its application (Sec. 3), we describe recent extensions and selected applications of the theory: Application to multiferroic materials (Sec. 4), to unconventional superconductors and liquid-crystal systems (Sec. 5), to reconstructive transitions (Sec. 6), and to the formation of the amorphous state (Sec. 7).

2. BASIC CONCEPTS OF THE LANDAU THEORY

2.1 Non-equilibrium free-energy and order-parameter

Let us introduce the basic concepts of the Landau theory through the example of a ferroelectric phase transition occurring at the critical temperature T_c in a crystal having a tetragonal paraelectric structure,

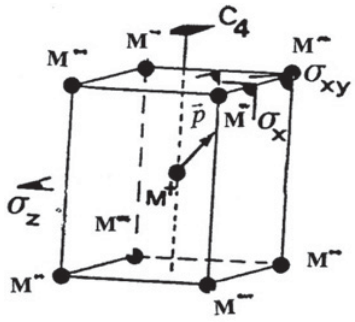

Figure 1. Unit-cell of the parent structure with tetragonal 4/*mmm* symmetry. $\vec{p}$ shows the displacement of the M^+ ion at the transition, while the M^- ions are not shifted.

Table 1. Transformation of the polarization components under the symmetry operations of the crystallographic point-group 4/*mmm*.

G_0	C_1	C_4	C_2	C_4^3	σ_x	σ_y	σ_{xy}	$\sigma_{\bar{x}y}$	I	S_4^3	σ_z	S_4	U_x	U_y	U_{xy}	$U_{\bar{x}y}$
P_z	P_z	P_z	P_z	P_z	P_z	P_z	P_z	P_z	$-P_z$	$-P_z$	$-P_z$	$-P_z$	$-P_z$	$-P_z$	$-P_z$	$-P_z$
P_x	P_x	P_y	$-P_x$	$-P_y$	$-P_x$	P_x	P_y	$-P_y$	$-P_x$	$-P_y$	P_x	P_y	P_x	$-P_x$	P_y	$-P_y$
P_y	P_y	$-P_x$	$-P_y$	P_x	P_y	$-P_y$	$-P_x$	P_x	$-P_y$	P_x	P_y	$-P_x$	$-P_y$	P_y	P_x	$-P_x$

denoted I, with 4/*mmm* point-group symmetry (Figure 1). Its vertices and its centre are respectively occupied by negative (M^-) and positive (M^+) ions. The ferroelectric phase II, stable below T_c, results from the displacement of the M^+ ions out of the centre of the cell, in an unspecified direction. As this displacement generates an electric dipole $\vec{p}$, phases I and II are characterized by $\vec{p} = 0$ and $\vec{p} \neq 0$, respectively, and at the macroscopic level by $\vec{P} = 0$ and $\vec{P} \neq 0$, where $\vec{P}$ is the electric polarization representing the sum of the dipoles over the unit volume.

The first concept of the Landau theory is that the I $\rightarrow$ II phase transition can be described by a non-equilibrium free-energy $F(T, \vec{P})$ expressed as a truncated Taylor expansion of the $\vec{P}$ components, the equilibrium values of the $\vec{P}$ components in the I and II phases corresponding to absolute minima of F with respect to the (P_x, P_y, P_z) variables. Such expansion is justified by the assumption of *continuity* of the phase transition in two different meanings: 1) The components vary continuously across T_c and therefore take small values close below T_c; 2) F is a continuous and derivable function of T and $\vec{P}$. The new idea is that F is *invariant* by the symmetry operations of the *parent* phase I and is therefore formed by invariant monomials of the $\vec{P}$ components. Table 1 shows the transformation of (P_x, P_y, P_z) by the symmetry operations of 4/*mmm*. One can verify that only quadratic $(P_z^2, P_x^2 + P_y^2)$ and higher *even*-degree monomials $(P_z^4, P_z^6, P_x^4 + P_y^4, P_x^2 P_y^2)$ remain invariants. Minimization of

$$F(T, \vec{P}) = F_0(T) + a_1 P_z^2 + a_2(P_x^2 + P_y^2) + ... \tag{1}$$

with respect to P_x, P_y and P_z yields the equations of state

$$\frac{\partial F}{\partial P_z} = 2a_1 P_z + ... = 0, \quad \frac{\partial F}{\partial P_x} = 2a_2 P_x + ... = 0, \quad \frac{\partial F}{\partial P_y} = 2a_2 P_y + ... = 0. \tag{2}$$

and the stability conditions

$$\frac{\partial^2 F}{\partial P_z^2} = 2a_1 + ... \geq 0, \frac{\partial^2 F}{\partial P_x^2} = 2a_2 + ... \geq 0, \quad \frac{\partial^2 F}{\partial P_y^2} = 2a_2 + ... \geq 0. \tag{3}$$

Equations (2) and (3) show that phase I ($\vec{P} = 0$) is stable for positive values of a_1 and a_2. Accordingly, phase II ($\vec{P} \neq 0$) can take place below T_c as a stable state only if a_1 or a_2 become negative. It means

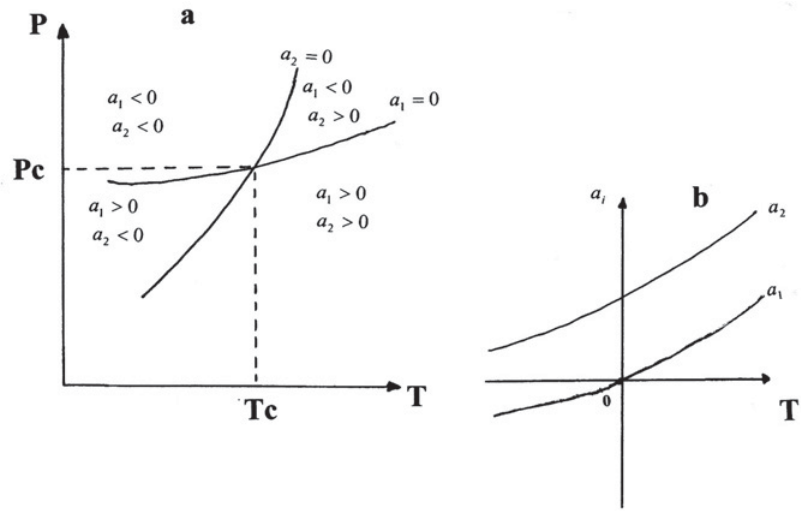

Figure 2. **(a)** Regions of the pressure-temperature plane corresponding to different signs of the phenomenological coefficients a_1 and a_2. **(b)** Figure illustrating the vanishing of the coefficient a_1 at a continuous transition while a_2 remains positive.

that one of these coefficients has to change its sign at the transition, i.e., a_1 or a_2 is equal to $a_0(T - T_c)$ with $a_0 > 0$. Here comes an important result of the Landau model: *Either* a_1 *or* a_2 *changes its sign at* $T = T_c$ *, but both coefficients cannot change their sign simultaneously*. It means that below T_c the M^+ ion can move either along the z axis or in the (x, y) plane but not in a general direction. This result stems from the property, illustrated by Figures 2(a) and 2(b), that a simultaneous vanishing at T_c of a_1 and a_2 should be observable at a *single point* of a two-dimensional (e.g. Temperature-Pressure) phase diagram (Fig. 2 (a)) and would lead to a ferroelectric state II, the symmetry of which would be modified by a vanishingly small variation of the external variables (temperature or pressure). Since the Landau model aims to describe a ferroelectric state stable within a finite range of temperature and pressure, one has to conclude that only one coefficient, let say a_1, changes it sign at T_c (Fig. 2 (b)), the other coefficient (a_2) remaining positive within a certain interval close to T_c. In this interval one has $a_2 = 0$ above *and* below T_c. Therefore the useful form of F reduces to

$$F(T, P_z) = F_0(T) + a_1 P_z^2 + b_1 P_z^4 + ... \tag{4}$$

Minimization of F truncated at the fourth-degree is expressed by the equations:

$$P_z(a_1 + 2b_1 P_z^2) = 0 \text{ and } a_1 + 6b_1 P_z^2 \geq 0 \tag{5}$$

which give the equilibrium values of P_z indicated in Fig. 3:

$$P_z^e = 0 \text{ for } T \geq T_c \text{ and}$$
$$P_z^e = \pm \left[\frac{a_0(T_c - T)}{2b_1} \right]^{1/2} \tag{6}$$

for $T < T_c$, under the condition $b_1 > 0$. The variable P_z whose equilibrium is zero above T_c and becomes non-zero below T_c is the transition *order-parameter*. The property that a single quadratic invariant coefficient (a_1) becomes negative at the transition can be formulated in group-theoretical terms, by considering the set of one and two-dimensional matrices given in Table 1, which transform as P_z and (P_x, P_y), respectively. These matrices form two among the *irreducible representations* of the 4/*mmm* point-group. Therefore, the Landau theory shows that *a continuous transition is induced by a single*

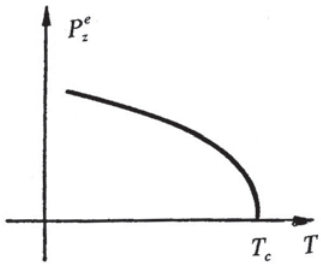

Figure 3. Temperature dependence of P_z^e, given by Eq. (6), across the transition.

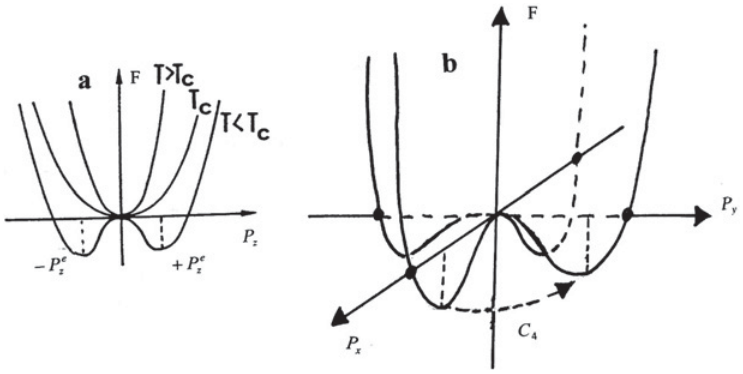

Figure 4. (a) Plot of $F(T, P_z) - F_0(T)$, given by Eq. (4), for three characteristic temperatures. **(b)** Plot of $F(T, P_x, P_y) - F_0(T)$, given by Eq. (7), for $T < T_c$.

irreducible representation of the parent symmetry group. The dimension of the matrices (here one or two) determines the *order-parameter dimensionality.*

2.2 Low-symmetry phases. Domains. Critical behaviour

A number of classical results of the Landau theory can be deduced from the preceding model:

1) Symmetry of the low-temperature phase is a subgroup G of the parent symmetry-group $G_0 = 4/mmm$, formed by the symmetry operations leaving invariant the order-parameter considered as a direction in a *vector space.* In the one-dimensional vector space P_z, Table 1 shows that $G = 4mm$. In the two-dimensional vector space (P_x, P_y) the invariant directions are $(P_x, 0), (P_y, 0)$, and $(P_x, P_y), (-P_x, P_y)$ with $P_x = P_y$, corresponding to absolute minima of the fourth-degree expansion:

$$F(T, P_x, P_y) = F_0(T) + a_2(P_x^2 + P_y^2) + b_2(P_x^2 + P_y^2)^2 + b_3 P_x^2 P_y^2 \tag{7}$$

and to the G-groups $2_x\,mm$, $2_y\,mm$, $2_{xy}\,mm$ and $2_{\bar{x}y}\,mm$.

2) The low-temperature states split into energetically equivalent *domains* of identical symmetries, the number of which is determined by the ratio between the order of G_0 (13) and the order of G (8 or 4). Therefore, *two* ferroelectric domains $(\pm P_z)$ coexist in the $G = 4mm$ state (Fig. 4(a)), whereas four domains (Fig. 4(b)) are found for each of the two classes of $mm2$ states $[(\pm P_x, 0), (0, \pm P_y)]$ and $[\pm P_{xy}, \pm P_{\bar{x}y}]$. The domains transform into one another by the symmetry operations lost at the $G_0 \rightarrow G$ symmetry change.

3) The critical behaviour of measurable physical properties related to first or second derivatives of F, can be obtained, namely (i) the order-parameter P_z given by Eq. (6), varying as $\approx (T_c - T)^{1/2}$

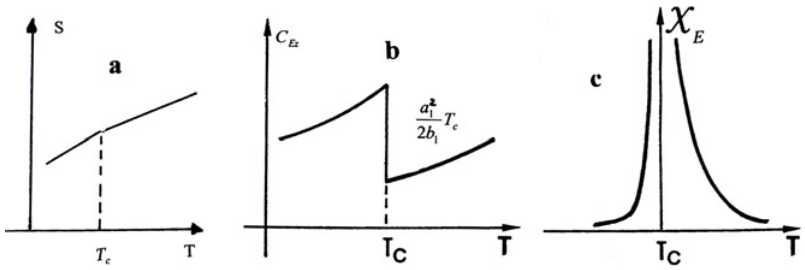

Figure 5. Critical behaviour at a second-order phase transition associated with the free-energy $F(T, P_z)$ for: **(a)** the entropy $S(T)$, **(b)** the specific heat $C_{Ez}(T)$ and **(c)** the dielectric susceptibility $\chi_E(T)$.

(Fig. 3), (ii) the entropy $S = -(\frac{\partial F}{\partial T})_{P_z}$ which displays no discontinuity at T_c (Fig. 5 (a)), implying zero latent heat $L = T_c \Delta S(T_c)$ at the transition, (iii) the specific heat $C_{E_z} = T\left(\frac{\partial S}{\partial T}\right)_{E_z}$ at constant field E_z conjugated to the order-parameter P_z, which undergoes an upward discontinuity at T_c (Fig. 5(b)), and (iv) the dielectric susceptibility $\chi = Lim_{E_z \to 0} \frac{\partial P_z}{\partial E_z}$ which diverges at T_c following the Curie-Weiss law (Fig. 5 (c)). The continuity across T_c of the physical quantities P_z and S, related to first derivatives of F, and the discontinuity of C_{E_z} and χ, corresponding to second derivatives of F, characterize *second-order phase transitions*, as defined by Ehrenfest [11].

2.3 Secondary order-parameters. Improper ferroelectric transitions

The preceding considerations have been restricted to the "primary" order-parameters, P_z or (P_x, P_y), the symmetry-breaking of which determines the essential properties of the phase transition at T_c, such as the symmetry of the stable state(s) which may arise below T_c, the domain pattern and the shape of the critical anomalies at the transition. Other physical quantities may arise below T_c, which do not modify the preceding properties but may influence secondary features of the phase diagram. In our introductory example, an eventual *deformation* of the unit-cell along z induced by the displacement of the M^+ ion, which is expressed by the strain-tensor component $e_{zz} = (z - z_0)/z_0$, constitutes an example of *secondary* (non-symmetry-breaking) order-parameter. In order to determine the influence of e_{zz} on the transition behaviour, one has to include in the free-energy F the lowest degree *coupling invariant* between e_{zz} and the primary order-parameter P_z as well as the elastic energy $\frac{1}{2}C_{33}e_{zz}^2$. F reads:

$$F(T, P_z, e_{zz}) = F(T, P_z) + c P_z^2 e_{zz} + \tfrac{1}{2} C_{33} e_{zz}^2 \tag{8}$$

Minimizing with respect to e_{zz} gives:

$$e_{zz}^e = -\frac{c}{C_{33}} P_z^2 = -\frac{c a_0}{2 b_1 C_{33}} (T_c - T) \tag{9}$$

below T_c, and $e_{zz}^e = 0$ for $T \geq T_c$ (Fig. 6. (a)). Replacing in Eq. (8) e_{zz} by its equilibrium value given by Eq. (9), one gets the renormalized free energy

$$F(T, P_z) = F_0(T) + a_1 P_z^2 + \left(b_1 - \frac{c^2}{2C_{33}}\right) P_z^4 \tag{10}$$

It shows that the secondary order-parameter e_{zz} renormalizes the fourth-degree coefficient. It therefore influences the limit of stability of the phases and the amplitude of the critical anomalies, but the phase diagram remains unchanged. The temperature dependences of e_{zz}^e, which varies *linearly* with $(T_c - T)$ (Fig. 6(a)), and of the elastic susceptibility $\mathrm{Lim}_{\sigma_{zz} \to 0} \frac{\partial e_{zz}}{\partial \sigma_{zz}}$, which undergoes a step-like jump at T_c (Fig. 6(b)), show that secondary order-parameters display a different critical behaviour than the primary order-parameter.

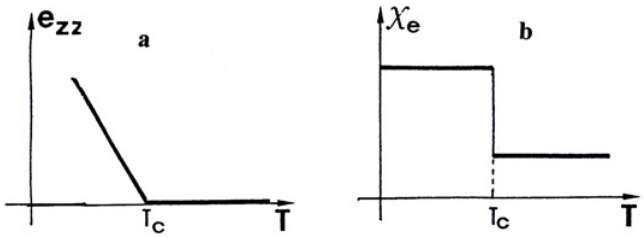

Figure 6. Temperature dependence of **(a)** the secondary order-parameter e_{zz} given by Eq. (9); **(b)** the corresponding elastic susceptibility χ_e.

In our introductory example, the electric polarization is the primary order-parameter since it is directly correlated to the symmetry-breaking transition mechanism consisting of the displacement of the M^+ ions. One deals here with a *proper* ferroelectric transition. However, the spontaneous polarization may also be a secondary order-parameter, the primary symmetry-breaking mechanism corresponding to a set of displacements inducing indirectly the formation of electric dipoles. In this case one speaks of an *improper* ferroelectric transition. This denomination is also used for *ferroelastic* transitions in which a spontaneous strain may constitute either the primary or the secondary order-parameter.

3. FIRST-ORDER TRANSITIONS. RULES GOVERNING THE APPLICATION OF THE LANDAU THEORY

3.1 First-order phase transitions

A large majority of the experimentally observed structural phase transitions are discontinuous [2]. When a group-subgroup relationship is preserved between the phases, discontinuous transitions can be nevertheless described theoretically, using the concepts introduced in Sec. 2 for continuous transitions. As a first example let us consider the free-energy given by Eq. (4), describing the paraelectric-ferroelectric transition I $\rightarrow$ II, in which the stability condition $b_1 > 0$ was assumed. For $b_1 < 0$ there exists for $T < T_c$, no stable minimum of F truncated at the fourth degree. Expanding F at the sixth degree

$$F(T, P_z) = F_0(T) + a_1 P_z^2 + b_1 P_z^4 + c_1 P_z^6 \tag{11}$$

and assuming $a_1(T - T_c), b_1 < 0$ and $c_1 > 0$, the equations minimizing F, which are

$$P_z(a_1 + 2b_1 P_z^2 + 3c_1 P_z^4) = 0 \ \text{ and } \ a_1 + 6b_1 P_z^2 + 15c_1 P_z^4 \geq 0 \tag{12}$$

provide the following description, summarized in Fig. 7, for the transition between phases I and II. For $T > T_2 = T_c + \frac{b_1^2}{3a_0c_1}$ phase I ($P_z^e = 0$) is the only stable phase. At $T = T_2$ phase II, corresponding to

$$P_z^e = \pm \left[\frac{-b_1 + \left(b_1^2 - 3a_0c_1(T - T_c)\right)^{1/2}}{3c_1} \right]^{1/2} \tag{13}$$

arises as a metastable state, associated with a secondary minimum in the non-equilibrium curve of $F(T, P_z) - F_0(T)$. On cooling the stability increases and phases I and II become equally stable at $T_1 = T_c + \frac{b_1^2}{4a_0c_1}$. Below T_1 phase I becomes metastable down to T_c where it becomes unstable. Therefore, discontinuous transitions are characterized by the following properties: 1) A *region of coexistence* between phases I and II in the temperature interval $\Delta T = T_2 - T_c = \frac{b_1^2}{3a_0c_1}$ in which the two phases are alternately metastable. The transition may occur at any temperature within the interval. However, the most probable transition temperature is T_1, corresponding to an equal stability for the two phases. The

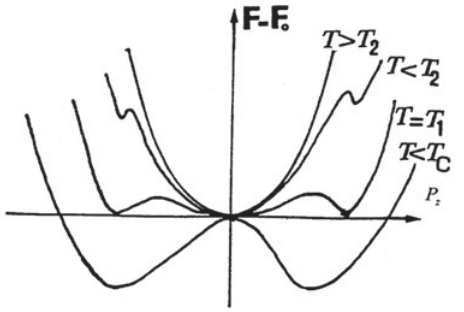

Figure 7. Temperature dependence of the non-equilibrium Landau expansion $F - F_0$ given by Eq. (11).

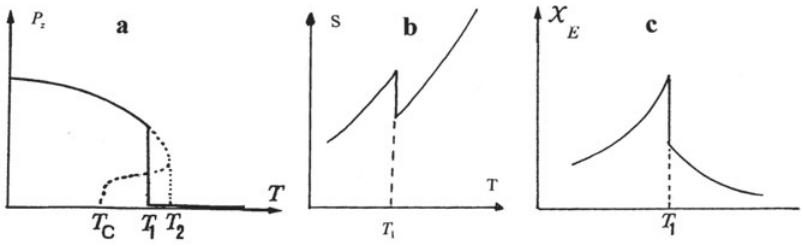

Figure 8. Temperature dependence of **(a)** the order-parameter, **(b)** the entropy and **(c)** the susceptibility associated with the order-parameter, across a first-order transition.

existence of a region of coexistence for the two phases implies a *thermal hysteresis* on cycling across the transition, i.e, the transition does not take place at the same temperature on cooling and heating. 2) A *discontinuous jump* $\Delta P_z^e(T_1) = (-\frac{b_1}{6c_1})^{1/2}$ of the equilibrium order-parameter P_z^e at the transition (Fig. 8(a)).

3) A *latent heat* at T_1 (Fig. 8(b)) which results from the order-parameter discontinuity, given by $L = T_1 \Delta S(T_1) = a_0 T_1 [\Delta P_z^e(T_1)]^2 = -\frac{a_0 b_1 T_1}{6c_1}$. As for P_z^e and S, a discontinuity will be also observed for all physical quantities related to first derivatives of F, such as the volume or the spontaneous strains. Therefore, discontinuous transitions are *first-order transitions* following Ehrenfest classification [11].

4) *Specific discontinuities* at T_1 for the physical quantities related to second derivatives of F. Figures 8(c) shows, for example, the temperature-dependence of the dielectric susceptibility, which undergoes a finite upward jump on cooling across T_1.

Figure 9 summarizes the phase diagram involving a second-order ($b_1 > 0$) and first-order ($b_1 < 0$) transitions. The cross-over between the two regimes occurs at a *tricritical point* corresponding to $b_1(T_c) = 0$ and $a_1(T_c) = 0$.

3.2 Integrity basis. Rule for truncating the Landau free-energy. Number of low-symmetry stable states

The Landau free-energy given by Eq. (4) or Eq. (11) can be expanded using a single invariant of the order-parameter $\Im = P_z^2$ and its successive powers $\Im^2, \Im^3, \ldots$ By contrast the free-energy defined by Eq. (7) requires two independent invariants $\Im_1 = P_x^2 + P_y^2$ and $\Im_2 = P_x^2 P_y^2$. $\Im$ and $(\Im_1, \Im_2)$ form the *integrity basis* associated with the order-parameters P_z and (P_x, P_y), respectively. In a more general way, the integrity basis associated with a given order-parameter is the set of independent invariant monomials which can be formed from the order-parameter components. The concept of integrity basis

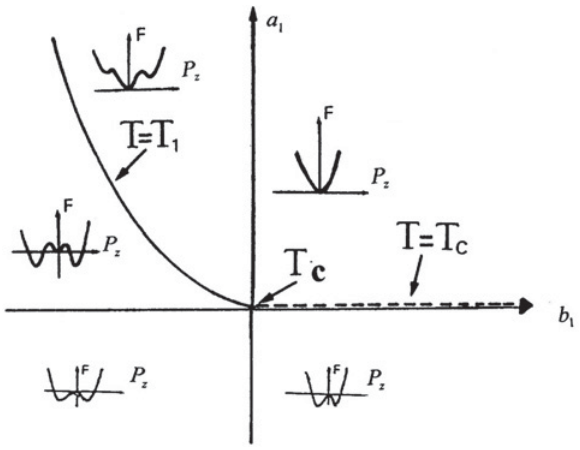

Figure 9. Phase-diagram in the (a_1, b_1) plane, corresponding to the Landau expansion given by Eq. (11). The tricritical point **Tc** separates the second-order transition line T = Tc from the first-order transition curve T = T$_1$. The temperature dependence of $F - F_0$ is shown in significant regions of the phase-diagram.

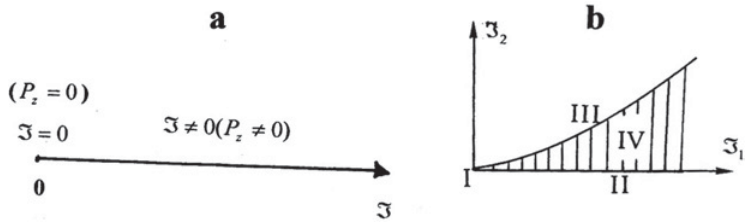

Figure 10. Orbit spaces associated with the order-parameters **(a)** P_z and **(b)** (P_x, P_y).

allows determining the *necessary degree* at which one has to expand a free-energy F in order to disclose, from the minimization of F, the *full set of stable states* associated with a given order-parameter.

Rule 1*: If n is the highest-degree of the monomials forming the integrity basis, one has to truncate the free-energy at the degree 2n for a second-order transition from the parent phase, and at the degree 2n+2 for a first-order transition.*

In the case of $F(P_z)$, $n = 2$ and F has to be expanded at the fourth-degree for a second-order transition (Eq. (4)), and at the sixth-degree for a first-order transition (Eq. (11)). For $F(P_x, P_y)$, $n = 4$ and F should be expanded at not less than the *eighth-degree.* Therefore, the fourth-degree at which the free-energy given by Eq. (7) is expanded does not account for the full set of stable states associated with the order-parameter (P_x, P_y). One can show that expanding $F(P_x, P_y)$ at the eighth-degree stabilizes an additional phase, corresponding to $P_x \neq P_y$ and to the lower symmetry m_z, associated with a general displacement of the M^+ ion in the (x, y) plane.

In order to predict the *number of stable states* N associated with a given order-parameter one can construct the phase diagram in the space of the order-parameter invariants (the *orbit-space*). Figures 10(a) and 10(b) show such phase diagrams for P_z and (P_x, P_y). One can verify that the stable states correspond to the origin (the parent phase), and to curves and surfaces of the orbit space (the low symmetry states) merging at the origin.

Rule 2*: The low-symmetry stable state associated with a given order-parameter corresponds to curves merging at the origin of the orbit-space, to surfaces limited by the curves, and to volumes limited by the*

surfaces. Surfaces are associated with subgroups of the limiting curves, and volumes to subgroups of the limiting surfaces.

The preceding rule applies straightforwardly when the orbit space has a dimension $m \leq 3$. For $m > 3$ one deals with hyper-surfaces and hyper-volumes and it is more practical to consider projections (*cuts*) of the orbit-space on two-or-three-dimensional spaces. In the particular case where m is equal to the order-parameter dimensionality n ($m = n$), the total number of stable states for groups generated by reflexions is $N = 2^n$. This is the case for the P_z and (P_x, P_y) order parameters for which one has, respectively, $m = n = 1$, and $m = n = 2$. Therefore the number of stable states are respectively $N = 2$ and $N = 2^2 = 4$.

3.3 Dependence of the phenomenological coefficients on external variables

In the free-energies $F(T, P_z)$ and $F(T, P_x, P_y)$ only one phenomenological coefficient, a_1 or a_2 corresponding to the quadratic invariants P_z^2 or $P_x^2 + P_y^2$, has been assumed to vary linearly and critically with temperature. The theoretical phase diagram resulting from a Landau model, shown for example in Fig. 9, is drawn in the space of the free-energy coefficients. In order that the theoretical phase diagram reflects the experimental phase diagram, one has to follow precise rules, deduced from the theory of Singularities [12], for determining the coefficients varying with external variables $(T, P, x, ...)$ and the form of their dependence on the external variables. 1) The number of varying coefficients should be equal to the number of external variables, i.e., one-two-or-three dimensional phase diagrams require a dependence of one-two-or-three coefficients, respectively, on the external variables. 2) Only the coefficients, whose sign determines the stability of the phases can be assumed to depend on the external variables. The remaining coefficients remain constant. 3) The coefficient of the highest degree invariant in the free-energy is always a positive constant. 4) The coefficient of the quadratic invariant depends linearly and critically on the external variable inducing the transition (e.g; the temperature). Such linear dependence ensures that the experimental phase diagram can be deduced from the theoretical phase diagram by a linear transformation preserving its singularities. However, the preceding coefficient, as well as coefficients of higher power invariants may depend nonlinearly on the other external variables (e.g. pressure or concentration). The non-linear dependence may involve integer or fractional powers of the external variables.

According to the preceding rules, the phase diagram associated with $F(T, P_z)$ expanded at the fourth-degree (Eq. (4)) is necessarily one dimensional, since b_1 is a positive constant, and a_1 can be assumed to vary in function of the single external variable T. Expanding $F(T, P_z)$ at the sixth-degree (Eq. (11)) allows constructing the two-dimensional phase diagram of Fig. 9. Assuming $c_1 > 0$, one can simply take $a_1 = a_0(T - T_c)$ and $b_1 = b_0(P - P_c)$ $(a_0 > 0, b_0 > 0)$ for preserving the main topological features of the theoretical phase diagram in the Temperature-Pressure phase diagram, namely, a parabolic shape for the first-order transition curve $T_1(P) = T_c + \frac{b_0^2(P-P_c)^2}{4a_0c_1}$ and a tricritical point at $T_1(P_c) = T_c$.

Figures 11(a)–(c) show different two-dimensional phase diagrams associated with the (P_x, P_y) order-parameter for an eighth-degree expansion:

$$F(T, P, P_x, P_y) = F_0(T, P) + a_1\Im_1 + a_2\Im_1^2 + a_4\Im_1^4 + b_1\Im_3 + b_2\Im_3^2 + c_{13}\Im_1\Im_3 \qquad (14)$$

where $\Im_1 = P_x^2 + P_y^2$ and $\Im_3 = \Im_1^2 - 8\Im_2$, with $\Im_2 = P_x^2 P_y^2$. One can verify that the topological features of the phase diagram associated with a given order-parameter can be modified depending on the signs and values of the phenomenological coefficients. However, a number of features are preserved, which can be foreseen from the topology of the phase-diagram in the orbit space (Fig. 10(b)), as for example the existence of four distinct phases, the region of stability of the lower symmetry phase IV, which is always found between phases II and III, or the property of phases II and III to be reached directly from phase I across a second-or-first-order transition line. Note that in the free-energy expansion, given by

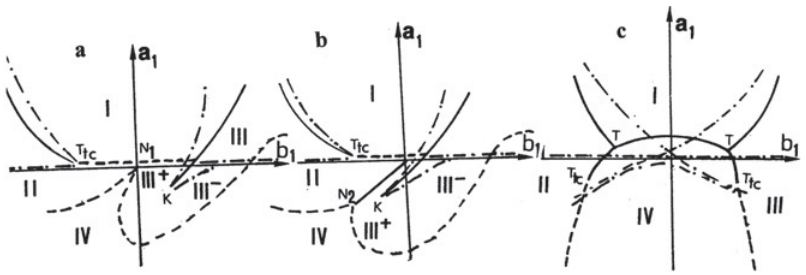

Figure 11. Phase diagrams in the (a_1, b_1) plane, associated with the eighth-degree expansion given by Eq. (14), corresponding to **(a)** $a_4 < 8b_2, c_{13} > 0$ and $\frac{c_{13}^2}{4b_2} < a_2 < \frac{c_{13}^2}{32a_4}$; **(b)** $c_{13} > 0$ and $0 < a_2 < \frac{c_{13}^2}{4b_2}$; **(c)** $a_2 < 0$ and $4a_2b_2 < c_{13}^2$. Dashed, full, and dashed-dotted curves correspond, respectively, to second-order, first-order, and limit of stability curves.

Table 2. Set of matrices associated with the three-dimensional irreducible representation T_{2u} of the $Pm\bar{3}m$ space-group at the centre of the primitive-cubic Brillouin-zone.

C_1	U_x	U_y	U_z	C_3^{2xyz}	$C_3^{xy\bar{z}}$	$C_3^{\bar{x}yz}$	$C_3^{x\bar{y}z}$	C_3^{xyz}	$C_3^{2x\bar{y}z}$	$C_3^{2xy\bar{z}}$	$C_3^{2\bar{x}yz}$
$\begin{pmatrix}1&0&0\\0&1&0\\0&0&1\end{pmatrix}$	$\begin{pmatrix}1&0&0\\0&-1&0\\0&0&-1\end{pmatrix}$	$\begin{pmatrix}-1&0&0\\0&1&0\\0&0&-1\end{pmatrix}$	$\begin{pmatrix}-1&0&0\\0&-1&0\\0&0&1\end{pmatrix}$	$\begin{pmatrix}0&1&0\\0&0&1\\1&0&0\end{pmatrix}$	$\begin{pmatrix}0&1&0\\0&0&-1\\-1&0&0\end{pmatrix}$	$\begin{pmatrix}0&-1&0\\0&0&1\\-1&0&0\end{pmatrix}$	$\begin{pmatrix}0&-1&0\\0&0&-1\\1&0&0\end{pmatrix}$	$\begin{pmatrix}0&0&1\\1&0&0\\0&1&0\end{pmatrix}$	$\begin{pmatrix}0&0&1\\-1&0&0\\0&-1&0\end{pmatrix}$	$\begin{pmatrix}0&0&-1\\1&0&0\\0&-1&0\end{pmatrix}$	$\begin{pmatrix}0&0&-1\\-1&0&0\\0&1&0\end{pmatrix}$

$U_{\bar{x}y}$	C_4^z	C_4^{3z}	U_{xy}	$U_{\bar{y}z}$	U_{yz}	C_4^x	C_4^{3x}	$U_{\bar{x}z}$	C_4^{3y}	U_{xz}	C_4^y
$\begin{pmatrix}0&-1&0\\-1&0&0\\0&0&-1\end{pmatrix}$	$\begin{pmatrix}0&-1&0\\1&0&0\\0&0&1\end{pmatrix}$	$\begin{pmatrix}0&1&0\\-1&0&0\\0&0&1\end{pmatrix}$	$\begin{pmatrix}0&1&0\\1&0&0\\0&0&-1\end{pmatrix}$	$\begin{pmatrix}-1&0&0\\0&0&-1\\0&-1&0\end{pmatrix}$	$\begin{pmatrix}-1&0&0\\0&0&1\\0&1&0\end{pmatrix}$	$\begin{pmatrix}1&0&0\\0&0&-1\\0&1&0\end{pmatrix}$	$\begin{pmatrix}1&0&0\\0&0&1\\0&-1&0\end{pmatrix}$	$\begin{pmatrix}0&0&-1\\0&-1&0\\-1&0&0\end{pmatrix}$	$\begin{pmatrix}0&0&-1\\0&1&0\\1&0&0\end{pmatrix}$	$\begin{pmatrix}0&0&1\\0&-1&0\\1&0&0\end{pmatrix}$	$\begin{pmatrix}0&0&1\\0&1&0\\-1&0&0\end{pmatrix}$

I	σ_x	σ_y	σ_z	S_3^{2xyz}	$S_3^{xy\bar{z}}$	$S_3^{\bar{x}yz}$	$S_3^{x\bar{y}z}$	S_3^{xyz}	$S_3^{2x\bar{y}z}$	$S_3^{2xy\bar{z}}$	$S_3^{2\bar{x}yz}$
$\begin{pmatrix}-1&0&0\\0&-1&0\\0&0&-1\end{pmatrix}$	$\begin{pmatrix}-1&0&0\\0&1&0\\0&0&1\end{pmatrix}$	$\begin{pmatrix}1&0&0\\0&-1&0\\0&0&1\end{pmatrix}$	$\begin{pmatrix}1&0&0\\0&1&0\\0&0&-1\end{pmatrix}$	$\begin{pmatrix}0&-1&0\\0&0&-1\\-1&0&0\end{pmatrix}$	$\begin{pmatrix}0&-1&0\\0&0&1\\1&0&0\end{pmatrix}$	$\begin{pmatrix}0&1&0\\0&0&-1\\1&0&0\end{pmatrix}$	$\begin{pmatrix}0&1&0\\0&0&1\\-1&0&0\end{pmatrix}$	$\begin{pmatrix}0&0&-1\\-1&0&0\\0&-1&0\end{pmatrix}$	$\begin{pmatrix}0&0&-1\\1&0&0\\0&1&0\end{pmatrix}$	$\begin{pmatrix}0&0&1\\-1&0&0\\0&1&0\end{pmatrix}$	$\begin{pmatrix}0&0&1\\1&0&0\\0&-1&0\end{pmatrix}$

$\sigma_{\bar{x}y}$	S_4^{3z}	S_4^z	σ_{xy}	$\sigma_{\bar{y}z}$	σ_{yz}	S_4^{3x}	S_4^x	$\sigma_{\bar{x}z}$	S_4^y	σ_{xz}	S_4^{3y}
$\begin{pmatrix}0&1&0\\1&0&0\\0&0&1\end{pmatrix}$	$\begin{pmatrix}0&1&0\\-1&0&0\\0&0&-1\end{pmatrix}$	$\begin{pmatrix}0&-1&0\\1&0&0\\0&0&-1\end{pmatrix}$	$\begin{pmatrix}0&-1&0\\-1&0&0\\0&0&1\end{pmatrix}$	$\begin{pmatrix}1&0&0\\0&0&1\\0&1&0\end{pmatrix}$	$\begin{pmatrix}1&0&0\\0&0&-1\\0&-1&0\end{pmatrix}$	$\begin{pmatrix}-1&0&0\\0&0&1\\0&-1&0\end{pmatrix}$	$\begin{pmatrix}-1&0&0\\0&0&-1\\0&1&0\end{pmatrix}$	$\begin{pmatrix}0&0&1\\0&1&0\\1&0&0\end{pmatrix}$	$\begin{pmatrix}0&0&1\\0&-1&0\\-1&0&0\end{pmatrix}$	$\begin{pmatrix}0&0&-1\\0&1&0\\-1&0&0\end{pmatrix}$	$\begin{pmatrix}0&0&-1\\0&-1&0\\1&0&0\end{pmatrix}$

Eq. (14), a number of high-degree invariants have been neglected, such as $\Im_1^3$ or $\Im_1^2\Im_3$, which can be shown to modify non-essential aspects of the phase diagrams, as the shape of the transition lines or the width of the metastability regions. Here, Pressure-Temperature phase diagrams can be deduced from the theoretical phase diagrams by assuming a linear temperature and pressure dependence for a_1 and b_2, while the other coefficients remain constant.

3.4 Application to Barium titanate

Let us illustrate the theoretical considerations presented in the preceding sections by the concrete example of Barium titanate. The parent phase of $BaTiO_3$ corresponds to the cubic perovskite structure of symmetry $Pm\bar{3}m$. The order-parameter associated to the sequence of ferroelectric phases [13] $Pm\bar{3}m \rightarrow 120^\circ\text{C} \rightarrow P4mm \rightarrow 5^\circ\text{C} \rightarrow Amm2 \rightarrow -90^\circ\text{C} \rightarrow R3m$ is formed by the three components (P_x, P_y, P_z) of the polarization, which span a three-dimensional irreducible representation (denoted T_{2u}) of the $Pm\bar{3}m$ space-group, at the centre of the primitive-cubic Brillouin-zone. Table 2 gives the 48 matrices corresponding to the *image-group* (the set of distinct matrices) of T_{2u}. From the transformation

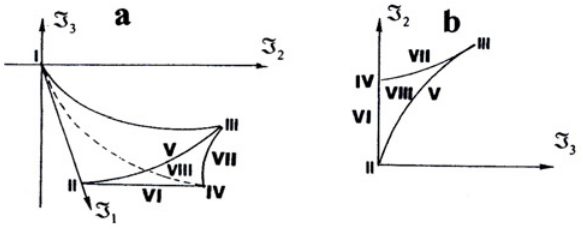

Figure 12. Topology of **(a)** the orbit space $(\Im_1, \Im_2, \Im_3)$ of Barium titanate deduced from Fig. 13, and **(b)** cross-section $(\Im_2, \Im_3)$ of the orbit space.

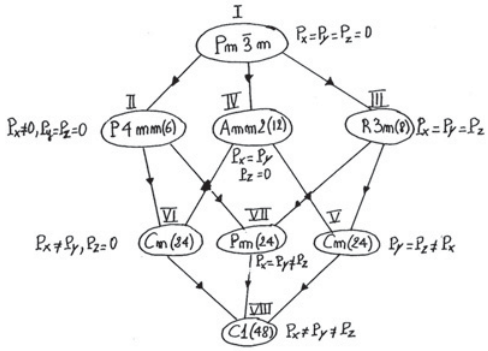

Figure 13. Symmetry relationship between the possible stable states associated with the three-component order-parameter inducing the ferroelectric transitions in $BaTiO_3$. The equilibrium values of the polarization components and the number of ferroelectric domains are indicated for each stable state.

properties of these matrices, the following independent invariants, forming the integrity basis of T_{2u}, can be constructed: $\Im_1 = P_x^2 + P_y^2 + P_z^2, \Im_2 = P_x^4 + P_y^4 + P_z^4$ and $\Im_3 = P_x^2 P_y^2 P_z^2$. Since the number of invariants m=3 is equal to the dimensionality n = 3 of the order-parameter, the number of distinct stable states permitted by the symmetry of the order-parameter is $2^3 = 8$. Figure 12 shows the location of the phases in the orbit spaces $(\Im_1, \Im_2, \Im_3)$ and $(\Im_2, \Im_3)$. Figure 13 summarizes the space-group symmetries of the phases, the corresponding invariant directions in the three-dimensional order-parameter space, which can be obtained from the matrices of T_{2u}, and the number of ferroelectric domains for each low-symmetry phase. In addition to the three ferroelectric phases reported in $BaTiO_3$, four lower symmetry phases having the symmetries Pm, Cm or $C1$ display regions of stability in the phase diagram. In order to obtain the full set of stable phases, the free-energy should be expanded at not less than the twelfth degree. Neglecting a number of high-degree invariants, one can take:

$$F(T, P, P_x, P_y, P_z) = F_0(T, P) + a_1\Im_1 + a_2\Im_1^2 + a_3\Im_1^3 + a_4\Im_1^4 + b_1\Im_2 + b_2\Im_2^2 + d_1\Im_3 + c_{12}\Im_1\Im_2 + c_{13}\Im_1\Im_3 + c_{112}\Im_1^2\Im_2 + d_2\Im_3^2 \quad (15)$$

When F is truncated at the sixth degree, the theoretical phase diagram contains the three ferroelectric phases actually found in $BaTiO_3$ (Fig. 14(a)), or only two of them (Fig. 14(b)). An eighth-degree expansion allows stabilization of one more phase of Cm (Fig. 14(c)) or Pm (Fig. 14(d)) symmetry. Only a twelfth-degree expansion permits the full set of low-symmetry phases to be stabilized. The corresponding three-dimensional phase diagram, shown in Fig. 15, requires three varying external variables.

The *proper* paraelectric-ferroelectric transitions in Barium titanate are also *improper* ferroelastic transitions, the spontaneous strains corresponding to secondary order-parameters. This can be foreseen by the number of ferroelastic domains arising in each phase, which corresponds to *half* of the number

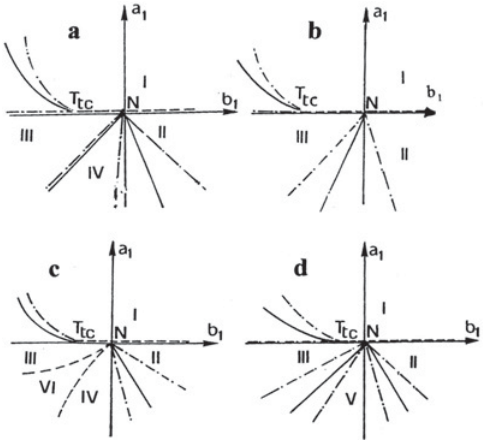

Figure 14. Selected phase diagrams in the (a_1, b_1) plane, associated with the Landau expansion given by Eq. (15) truncated at the sixth degree (Figures **(a)** and **(b)**) and at the eighth degree (Figures **(c)** and **(d)**).

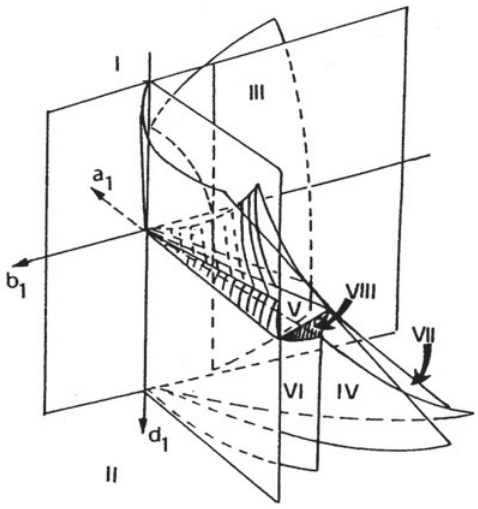

Figure 15. Three-dimensional phase-diagram in (a_1, b_1, d_1) space, corresponding to the twelve-degree expansion given by Eq. (15).

of ferroelectric domains. For example, the tetragonal $P4mm$ phase displays six ferroelectric domains, corresponding to $\pm P_x, \pm P_y$ and $\pm P_z$. Each pair of ferroelectric domains is coupled to a single ferroelastic domain, as shown in Fig. 16, via the coupling invariants: $P_z^2(2e_{zz} - e_{xx} - e_{yy})$, $P_y^2(2e_{yy} - e_{zz} - e_{xx})$ and $P_x^2(2e_{xx} - e_{yy} - e_{zz})$.

4. PHASE TRANSITIONS INDUCED BY SEVERAL ORDER-PARAMETERS: THEORY OF MAGNETIC MULTIFERROICS

4.1 Phase diagrams associated with a reducible order-parameter

The transitions examined in the preceding sections were related to a single *irreducible* order-parameter, in agreement with the essential statement of the Landau theory which associates a phase transition to a single irreducible representation. There exist, however, experimentally observed phase transitions which

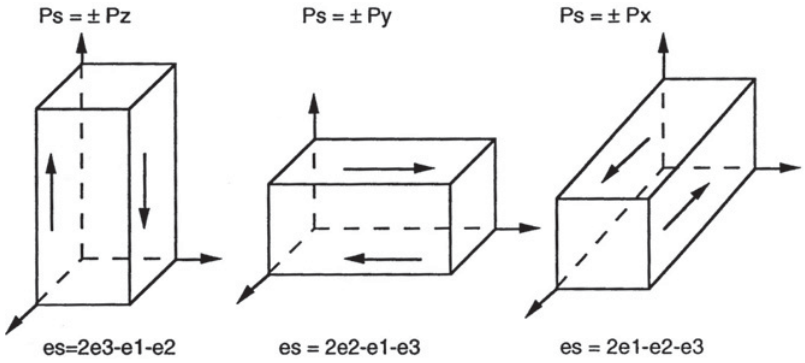

Figure 16. Configuration of the unit-cell for the six ferroelectric domains and three ferroelastic domains associated with the $P4mm$ phase of $BaTiO_3$. Ps and es denote the corresponding spontaneous polarization and strain.

have to be connected to more than one irreducible order-parameter. Referring to Fig. 2(b), two main situations can be met: 1) The transition associated with the P_z order-parameter occurs discontinuously at $T_1 > T_c$ and triggers the vanishing of the a_2 coefficient at T_1, giving rise below T_1 to a phase displaying non-zero equilibrium values of P_z *and* (P_x, P_y). The symmetry of this phase corresponds to the intersection of the symmetries induced by both order-parameters. Such situation, first described by Holakovsky [14], is found in a number of structural transitions. 2) Another situation, described by Lifshitz [15], corresponds to a sequence of two successive second-order transitions taking place consecutively at T_{c1} and T_{c2}. The first transition at T_{c1}, corresponds to the vanishing of a_1, with the spontaneous onset of a P_z component, whereas the second transition at T_{c2} gives rise to spontaneous values of (P_x, P_y). The symmetry of the phase arising below T_{c2} will reflect the coupling of both order-parameters P_z and (P_x, P_y), although only one symmetry breaking mechanism associated with (P_x, P_y) is involved. This situation, which is realized in a number of magnetic multiferroic compounds, is described in the following subsections.

4.2 Theoretical description of the sequence of phase transitions in $MnWO_4$

4.2.1 Phenomenological description at zero magnetic field

As a first illustrative example of transition induced by coupled order-parameters let us describe the sequence of magnetic phases occurring in $MnWO_4$. Below its wolframite-type structure of monoclinic $P2/c$ symmetry, $MnWO_4$ undergoes three successive magnetic transitions [16, 17] at 13.5 K (T_N), 12.7 K (T_2) and 7.6 K (T_1). They lead, respectively, to an incommensurate antiferromagnetic phase (AF3), an incommensurate elliptical spiral phase (AF2) displaying an electric polarization $\vec{P}//b$, and a commensurate antiferromagnetic phase (AF1). The transition wave-vectors are $\vec{k}_{inc} = (-0.214, \frac{1}{2}, 0.457)$ for AF2 and AF3, and

$$\vec{k}_{com} = \left(\pm\frac{1}{4}, \frac{1}{2}, \frac{1}{2}\right) \text{ for AF1.}$$

At variance with structural transitions which are induced by irreducible representations of crystallographic space-groups, magnetic transitions are induced by irreducible *corepresentations* of *magnetic* space-groups [18]. In the present case, the parent phase is the paramagnetic gray space-group $P2/c1'$, which is formed by the symmetry operations of $P2/c$ plus their combination with the time-reversal symmetry operation T. Since the spin-densities considered in the Landau approach to magnetic phase transitions are *macroscopic* (average) *non-quantum* objects, T is simply represented by

Table 3. Generators of the irreducible corepresentations Γ^{k1} and Γ^{k2} of the $P2/c1'$ paramagnetic space-group, deduced from the irreducible representations $\widehat{\tau}_1$ and $\widehat{\tau}_2$ of $G_k = m_y$, given in Kovalev's tables [19], for k_{inc} and k_{com}. T is the time-reversal symmetry. For AF2 and AF3, $\varepsilon \approx 0.457\pi, \varepsilon_1 \approx 0.418\pi$ and $\varepsilon_2 = 2\varepsilon$. For AF1, $\varepsilon = \varepsilon_1 = \pi/2$ and $\varepsilon_2 = \pi$.

$P2/c1'$		$(\sigma_y\|00\frac{c}{2})$	$(I\|000)$	T	$(E\|a00)$	$(E\|0b0)$	$(E\|00c)$
Γ^{k1}	$\bar{S}_1$	$\begin{pmatrix} e^{i\varepsilon} & \\ & e^{-i\varepsilon} \end{pmatrix}$	$\begin{pmatrix} 1 & \\ & 1 \end{pmatrix}$	$\begin{pmatrix} -1 & \\ & -1 \end{pmatrix}$	$\begin{pmatrix} e^{i\varepsilon_1} & \\ & e^{-i\varepsilon_1} \end{pmatrix}$	$\begin{pmatrix} -1 & \\ & -1 \end{pmatrix}$	$\begin{pmatrix} e^{i\varepsilon_2} & \\ & e^{-i\varepsilon_2} \end{pmatrix}$
	$\bar{S}_1{}^*$						
Γ^{k2}	$\bar{S}_2$	$\begin{pmatrix} -e^{i\varepsilon} & \\ & -e^{-i\varepsilon} \end{pmatrix}$	$\begin{pmatrix} 1 & \\ & 1 \end{pmatrix}$	$\begin{pmatrix} -1 & \\ & -1 \end{pmatrix}$	$\begin{pmatrix} e^{i\varepsilon_1} & \\ & e^{-i\varepsilon_1} \end{pmatrix}$	$\begin{pmatrix} -1 & \\ & -1 \end{pmatrix}$	$\begin{pmatrix} e^{i\varepsilon_2} & \\ & e^{-i\varepsilon_2} \end{pmatrix}$
	$\bar{S}_2{}^*$						

the matrix $-I$, where I is the identity matrix. Therefore the irreducible corepresentations of $P2/c1'$ are simply deduced from the corresponding irreducible representations of $P2/c$, as shown in Table 3, by adding a set of matrices obtained by multiplying the matrices of the relevant irreducible representations of $P2/c$ by $-I$. Taking into account the symmetry group $G_k = m_y$ of $\vec{k}_{inc}$ and $\vec{k}_{com}$ one gets two relevant two-dimensional irreducible corepresentations [19], denoted Γ^{k1} and Γ^{k2}, whose generators are given in Table 3. The complex amplitudes transforming according to Γ^{k1} and Γ^{k2} are denoted $\bar{S}_1 = S_1 e^{i\theta_1}, \bar{S}_1^* = S_1 e^{-i\theta_1}$ and $\bar{S}_2 = S_2 e^{i\theta_2}, \bar{S}_2^* = S_2 e^{-i\theta_2}$. For $\vec{k} = \vec{k}_{inc}$ the order-parameter invariants $\Im_1 = S_1^2, \Im_2 = S_2^2$ and $\Im_3 = S_1^2 S_2^2 \cos 2\varphi$, with $\varphi = \theta_1 - \theta_2$ yield the Landau expansion

$$\Phi_1(T, S_1, S_2, \varphi) = \Phi_{10}(T) + \frac{\alpha_1}{2}\Im_1 + \frac{\beta_1}{4}\Im_1^2 + \frac{\alpha_2}{2}\Im_2 + \frac{\beta_2}{4}\Im_2^2 + \frac{\gamma_1}{2}\Im_3 + \frac{\gamma_2}{4}\Im_3^2 \tag{16}$$

which has to be expanded up to the degree $2n = 8$ since the degree of $\Im_3$ is $n = 4$. Minimizing with respect to φ gives

$$S_1^2 S_2^2 \sin 2\varphi(\gamma_1 + \gamma_2 S_1^2 S_2^2 \cos 2\varphi) = 0 \tag{17}$$

Eq. (17) and the minimization of Φ_1 with respect to S_1 and S_2 show that *five* distinct stable states, denoted I-V, may arise below the paramagnetic (P) phase for different equilibrium values of S_1, S_2 andφ. This can be foreseen from the phase diagram in the orbit-space shown in Fig. 17(a) which contains two curves, two surfaces limited by the curves and the volume limited by the surfaces. Theoretical phase diagrams showing the location of the phases can be constructed in the two dimensional spaces (α_1, α_2) and $(\alpha_2 - \alpha_1, \gamma_1)$ (Figs. 17(b) and 17(c)), and in the three-dimensional space $(\alpha_1, \alpha_2, \gamma_1)$ (Fig. 17(d)). Since the AF2 and AF3 phases possess incommensurate structures one can only determine their magnetic *point-groups*. On that goal one cannot use, as for commensurate structures, the matrices of the irreducible corepresentations for disclosing the invariant directions in the order-parameter space. The procedure for determining the macroscopic (point-group) symmetries of incommensurate phases was given by Dvorak et al [20]. In particular, one can use here the following useful rules: 1) When the phase of the order-parameter (here θ_1, θ_2 or φ) can be shifted without modifying the stability of the incommensurate structure, its point-group coincides with the point-group G_P of the parent structure (here the paramagnetic point-group $2/m1'$), 2) If the phase of the order parameter is fixed, the point-group symmetry of the incommensurate structure is a subgroup of G_P formed by the symmetry elements preserving the *spontaneous* macroscopic physical tensor components induced by a coupling with the order-parameter (i.e. here, components of the magnetization $\vec{M}$ and electric polarization $\vec{P}$). Figure 18 gives the magnetic point-group symmetries of the five phases which may stabilize below the paramagnetic phase. They correspond to *gray* magnetic point-groups associated with antiferromagnetic structures.

Neutron diffraction data [21] show that the AF3 phase is induced by Γ^{k2}, coinciding with phase I in Fig. 17, with $S_1 = 0$ and $S_2 \neq 0$. It has the magnetic point-group $2_y/m_y1'$ involving a doubling of the b-lattice parameter and an incommensurate modulation of the spin-density in the (x, z) plane. The AF2 spiral phase, induced by $\Gamma^{k1} + \Gamma^{k2}$ identifies to phase II in Fig. 17, corresponding to $S_1 \neq 0, S_2 \neq 0$,

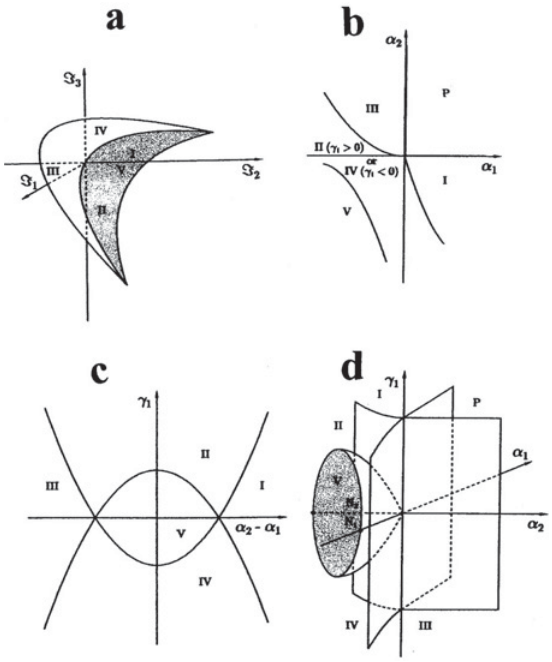

Figure 17. Phase diagrams at zero magnetic field deduced from the minimization of Φ_1, given by Eq. (16) in **(a)** the orbit space $(\Im_1, \Im_2, \Im_3)$, **(b)** the (α_1, α_2) plane, **(c)** the $(\alpha_2 - \alpha_1, \gamma_1)$ plane, and **(d)** the $(\alpha_1, \alpha_2, \gamma_1)$ space. In **(d)** the phases are separated by second-order transition surfaces which become curves in **(b)** and **(c)**.

$\varphi = (2n+1)\frac{\pi}{2}$, and to the magnetic symmetry $2_y 1'$. The dielectric free-energy $\Phi_1^D = \delta P_y S_1 S_2 \sin\varphi + \frac{P_y^2}{2\varepsilon_{yy}^0}$ gives the equilibrium polarization

$$P_y^e = \pm\delta\varepsilon_{yy}^0 S_1^e S_2^e \tag{18}$$

which changes its sign for opposite senses of the spiral configuration, as observed experimentally [22]. The order-parameter $\bar{S}_2$, activated at the paramagnetic→AF3 transition, is frozen at the AF3→AF2 transition. Therefore, Eq. (3) expresses a *linear* dependence of P_y on $\bar{S}_1$. In the AF3 and AF2 phases Φ_1 can be truncated at the fourth-degree. Putting $\alpha_1 = a_1(T - T_0)$ and $\alpha_2 = a_2(T - T_N)$ one finds that P_y varies in the AF2 phase as

$$P_y^e(T) = \pm A(T_2 - T)^{1/2} \tag{19}$$

with $A = \delta\varepsilon_{yy}^0 \left[\frac{a_2(a_2\gamma_1 + a_1\beta_2)}{\beta_2(\beta_1\beta_2 - \gamma_1^2)(T_N - T_2)}\right]^{1/2}$. The dielectric permittivity follows a Curie-Weiss-type law

$$\varepsilon_{yy}(T) = \left(1 - C\frac{T_N - T}{T - T_2}\right)(T > T_2), \text{ and } \varepsilon_{yy}(T) = \left(1 - D\frac{T_N - T}{T_2 - T}\right)(T < T_2) \tag{20}$$

with $C = \frac{\varepsilon_{yy}^0 a_2 \delta^2}{a_2\gamma_1 + a_1\beta_2}$, and $D = C\frac{\gamma_1^2 - \beta_1\beta_2}{\gamma_1^2 - 4\beta_1\beta_2}$. Figure 19 shows the excellent fit of $P_y^e(T)$ and $\varepsilon_{yy}(T)$ with the experimental curves. The low value of $\approx 40\,\mu\text{C/m}^2$ found for P_y at 10 K, reflects the hybrid character of the ferroelectricity in spiral magnets: The critical anomalies are typical of a *proper* ferroelectric transition, while the magnitude of the polarization is of the order found in *improper* ferroelectrics.

Neutron diffraction results [21] indicate that the transition to the commensurate AF1 phase triggers a decoupling of $\bar{S}_1$ and $\bar{S}_2$. The lock-in at T_1, induced by Γ^{k2}, gives rise to the invariant $\Im_4 = S_2^4 \cos 4\theta_2$.

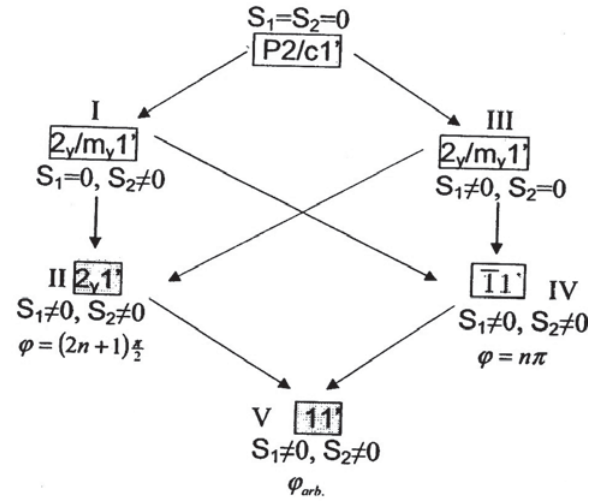

Figure 18. Connections between the magnetic point-groups of phases I-V induced by $\Gamma^{k1} + \Gamma^{k2}$ and equilibrium conditions fulfilled by the order-parameters involved in $MnWO_4$, in each phase.

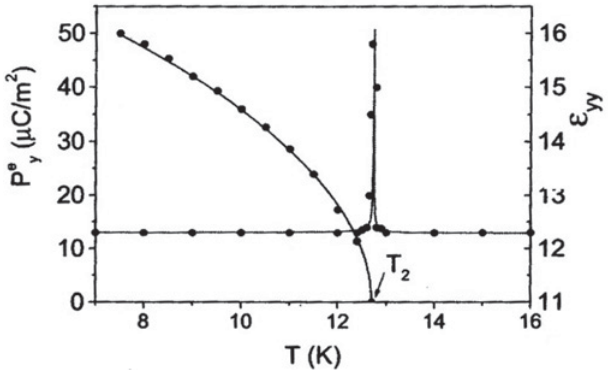

Figure 19. Fit of the temperature dependences of the spontaneous polarization $P_y^e(T)$ (Eq. (19)) and dielectric permittivity $\varepsilon_{yy}(T)$ (Eq. (20)) with the experimental points from Taniguchi et al [16].

The Landau expansion associated with the transition to AF1 is

$$\Phi_2(T, S_2, \theta_2) = \Phi_{20}(T) + \frac{\alpha'}{2} S_2^2 + \frac{\beta'}{4} S_2^4 + \frac{\gamma_1'}{4} S_2^4 \cos 4\theta_2 + \frac{\gamma_2'}{8} S_2^8 \cos^2 4\theta_2 \tag{21}$$

The equations of state show that three commensurate phases, denoted I'-to III', displaying a fourfold unit-cell ($\vec{b} + \vec{c}, \vec{c} - \vec{b}, 2\vec{a} + \vec{c}$), may appear below T_1. The AF1 phase identifies to phases I' or II', stable for $\cos 4\theta_2^e = \pm 1$, both described by the magnetic space group $C_a 2/c$ (see the chapter by Rodríguez-Carvajal and Bourrée for the notation of magnetic space groups). Phase III', stable for $\cos 4\theta_2^e = \frac{\gamma_1' \beta'^2}{\gamma_2' \alpha'^2}$, has the symmetry $C_a c$.

4.2.2 Magnetic field induced effects

The AF1, AF2 and AF3 order-parameter symmetries allow describing the magnetoelectric effects [16, 17, 22] observed in $MnWO_4$. Let us first note the following: 1) Since the magnetic symmetries of the

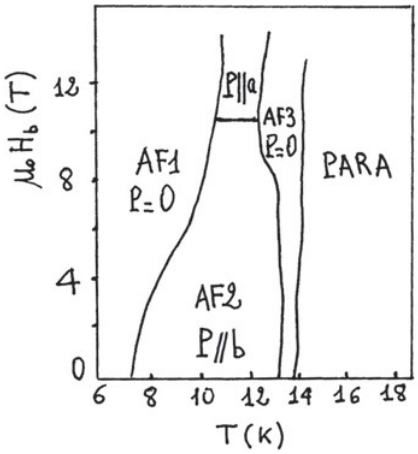

Figure 20. Magnetoelectric phase diagram of $MnWO_4$ in magnetic field parallel to the b axis, from Taniguchi et al [16].

ordered phases correspond to gray point-groups one can expect magnetic-field induced magnetoelectric effects, but not the reciprocal electric-field induced magnetoelectric effects, since the time-reversal symmetry forbids the existence of non-zero macroscopic components of the magnetization $\vec{M}$ under applied electric field. 2) When applying a magnetic field $\vec{B}$ to a phase, the magnetic symmetry of the phase may be lowered as it corresponds to the intersection of its symmetry group at $\vec{B} = 0$ with the symmetry group of the magnetic field.

Various magnetic field induced effects are observed in $MnWO_4$: 1) The region of stability of the AF2 phase decreases with respect to AF3 and AF1 with increasing B_y field (Fig. 20) and depends on the orientation of $\vec{B}_y$ with respect to the magnetic easy axis; 2) Above a threshold field B_y^{th} of about 10 T, the AF2 phase undergoes a polarization-flop transition $P_y \rightarrow P_x$; 3) Cycling across B_y^{th} and canting oppositely $\vec{B}$ with respect to the y axis, yields an opposite sign for P_x. The reduction of the stability range of AF2 with respect to AF3 and AF1 can be deduced from the equation expressing the stability of the AF2 phase under B_y field. Taking into account the magnetic free-energy $\Phi_1^M = \mu\frac{M^2}{2} - \vec{B}.\vec{M}$ and coupling invariants $\kappa_1 M_y^2 S_1^2$ and $\kappa_2 M_y^2 S_2^2$, the stability condition $\frac{\partial^2\Phi_1'}{\partial S_1^2}\frac{\partial^2\Phi_1'}{\partial S_2^2} - \left(\frac{\partial^2\Phi_1'}{\partial\varphi^2}\right)^2 \geq 0$, with $\Phi_1'(T, S_1, S_2, B_y) = \Phi_1(T, S_1, S_2) + \mu_{yy}^{-2} B_y^2(\kappa_1 S_1^2 + \kappa_2 S_2^2)$, yields

$$T_2(B_y) - T_2(0) = -\varepsilon\mu_{yy}^{-2} B_y^2 \tag{22}$$

where $\varepsilon = (\beta_1\kappa_1 + \gamma_1\kappa_2)(\beta_1\alpha_1 + \gamma_1\alpha_2)^{-1}$. For $\varepsilon < 0$ the stability range of the AF2 phase *decreases* with respect to AF3 under increasing B_y field. In a similar way the AF2 stability range reduces with respect to AF1, under B_y field. The polarization flop corresponds to *a first-order transition to phase III'*, *which displays a polarization component* P_x *and no* P_y *component*. Therefore, the threshold field B_y is given by the equality of the expansions

$$\Phi_1(T, S_1^e, S_2^e) - B_y^{th} M_y^{II} = \Phi_{II}(T, S_2^e) - B_y^{th} M_y^{III'} \tag{23}$$

Above B_y^{th} the AF2 phase switches to the high-field phase III', which symmetry $C_a c$ cancels P_y and gives rise to the polarization

$$P_x^{III'} = -\delta' \varepsilon_{xx}^0 S_2^{e^2} \sin 2\theta_2^e \tag{24}$$

deduced from the dielectric free-energy $\Phi_2^D = \delta' P_x S_2^2 \sin 2\theta_2 + \frac{P_x^2}{2\varepsilon_{xx}^0}$. Decreasing B_y below B_y^{th} switches back phase III' to AF2. If $\vec{B}$ is canted at an angle ϕ with respect to the b-axis in the (x, z) plane, the magnetoelectric coupling $\nu P_x M_x M_y S_1 S_2 \sin\varphi$ induces the polarization

$$P_x^e = -2\varepsilon_{yy}^0 \nu \mu_{yy}^{-2} B_y^2 S_1^e S_2^e \sin\varphi^e \sin 2\phi \tag{25}$$

Canting oppositely $\vec{B}$ from the b-axis ($\phi \to -\phi$) *reverses* P_x^e. Increasing again B_y above B_y^{th} yields an opposite sign for $P_x^{III'}$ in phase III', as observed by Taniguchi et al [23]. The AF2 stability range depends on the angle Ψ_0 of $\vec{B}$ and magnetic easy axis in the paramagnetic phase. This property relates to the anisotropy of the magnetic free-energy $\Phi_1^M = \frac{1}{2}\vec{M}\hat{\mu}\vec{M} - \vec{B}\vec{M}$, where $\hat{\mu}$ is the paramagnetic susceptibility tensor, with $\tan 2\Psi_0 = 2\mu_{xz}(\mu_{xx} - \mu_{zz})^{-1}$. If $\vec{B}$ is at an angle Ψ with the x-axis in the (x, z) plane, one finds

$$T_2(\Psi) - T_2 = \quad \varepsilon B^2 \left\{ 1 - \frac{td^{-1}}{2} \left[t - (t^2 - 4d)^{1/2} \cos 2(\Psi - \Psi_0) \right] \right\} \tag{26}$$

Where $t = \mu_{xx} + \mu_{zz}$ and $d = \mu_{xx}\mu_{zz} - \mu_{xz}^2$. For $\varepsilon < 0$ the AF2 stability range is maximum along the easy axis ($\Psi = \Psi_0$). It decreases when Ψ increases from Ψ_0 to $\Psi_0 + \frac{\pi}{2}$, reducing to the stability range at zero field if $\mu_{xz}, \mu_{xx} << \mu_{zz}$. Such variation has been observed in the AF2 phase, in which $\Psi_0 \cong 35^\circ$ coincides with the direction of the spins in the (x, z) plane. When $\vec{B}$ is at an azimuthal angle ψ with the (x, z) plane, the AF2 stability range decreases when ψ increases from $\psi = 0$ to $\psi = \pi/2$, as reported experimentally.

4.2.3 Microscopic origin of the unconventional ferroelectricity in magnetic multiferroics: The Dzialoshinskii-Moriya and symmetric interactions

Let us express the phenomenological order-parameters $\bar{S}_1$ and $\bar{S}_2$ in function of the magnetic spins in the commensurate phases I'-III'. Denoting $\mathbf{s}_1$-$\mathbf{s}_8$ the spins associated with the eight Mn^{2+} ions of the fourfold primitive monoclinic unit-cell (Fig. 21), one can write $\mathbf{s}_i = s_i^a \vec{a} + s_i^b \vec{b} + s_i^c \vec{c}$ $(i = 1 - 8)$, where $\vec{a}, \vec{b}$ and $\vec{c}$ are the monoclinic lattice vectors. Projecting the 24×24 matrices transforming the $s_i^{a,b,c}$-components on Γ^{k1} and Γ^{k2} gives

$$\bar{S}_1^{a,c} = L_1^{a,c} + iL_3^{a,c}, \;\; \bar{S}_1^b = -L_4^b + iL_2^b, \;\; \bar{S}_2^{a,c} = -L_4^{a,c} + iL_2^{a,c}, \;\; \bar{S}_2^b = L_1^b + iL_3^b \tag{27}$$

where the $\bar{S}_i^m (i = 1, 2 \quad m = a, b, c)$ represent different forms of $\bar{S}_1$ and $\bar{S}_2$. The $L_i^m (i = 1 - 4)$ are projections of the vectors $\mathbf{L}_1 = \mathbf{s}_1$-$\mathbf{s}_2$-$\mathbf{s}_7$+$\mathbf{s}_8$, $\mathbf{L}_2 = \mathbf{s}_1$-$\mathbf{s}_2$+$\mathbf{s}_7$-$\mathbf{s}_8$, $\mathbf{L}_3 = \mathbf{s}_3$-$\mathbf{s}_4$+$\mathbf{s}_5$-$\mathbf{s}_6$, and $\mathbf{L}_4 = \mathbf{s}_3$-$\mathbf{s}_4$-$\mathbf{s}_5$+$\mathbf{s}_6$. Table 4 summarizes the equilibrium values of the spin-components in phases I', II' and III' which correspond to $\bar{S}_1^{a,b,c} = 0$ and $\cos 4\theta_2^{a,b,c} = 1$ (I'), $\cos 4\theta_2^{a,b,c} = -1$ (II') and $\cos 4\theta_2^{a,b,c} \neq \pm 1$ (III'). Figures 21(a) and 21(b) represent the magnetic structures in the (x, z) plane for phases I' and II'. It shows that structure of phase II' *coincides with the antiferromagnetic order reported in the AF1 phase* of $MnWO_4$. The lack of spin components along $\vec{b}$ assumed for this phase may be due to their relativistic origin as suggested in Ref. [21]. The equilibrium values given for the spin components in Table 4, allow to determine the magnetic structure of Phase III', which identifies to the high-field phase of $MnWO_4$.

Other commensurate structures can take place for $\vec{k} = \vec{k}_{com}$ when the spin components associated with $\bar{S}_1$ and $\bar{S}_2$ order simultaneously. Two among these structures, denoted IV' ($\theta_1^e = 0, \theta_2^e = \pi/2$) and V' ($\theta_1^e = \pi/2, \theta_2^e = 0$), display the symmetry 2_y and the same form of $P_y = \frac{1}{2i}(\bar{S}_1\bar{S}_2^* - \bar{S}_2\bar{S}_1^*) = S_1 S_2 \sin\varphi$ as in the AF2 phase. Although these structures are not stabilized in $MnWO_4$ they represent lock-in limits of the incommensurate AF2 structure, and can be used for investigating the microscopic origin of ferroelectricity in the spiral magnetic structure. Since $\bar{S}_1$ and $\bar{S}_2$ are both realized by three

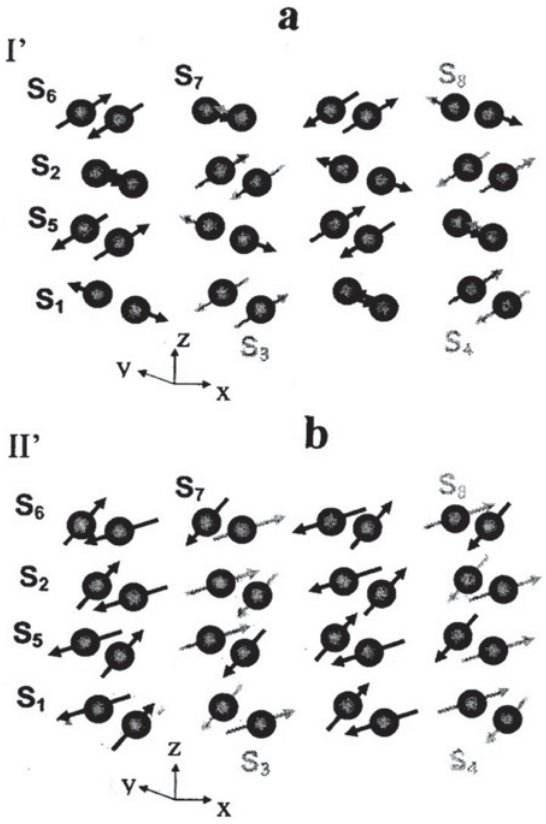

Figure 21. Projections on the (x, z) plane of the magnetic structures of **(a)** phase I' and **(b)** phase II' deduced from Table IV. The coordinates of the eight Mn^{2+} ions corresponding to the spins $\vec{s}_1 - \vec{s}_8$, in the primitive monoclinic unit-cell of the two structures, are for ion $1\left(\frac{1}{2}, y-1, \frac{5}{4}\right)$, $2\left(\frac{1}{2}, y, \frac{5}{4}\right)$, $3\left(\frac{3}{2}, y, \frac{5}{4}\right)$, $4\left(\frac{3}{2}, y, \frac{9}{4}\right)$, $5\left(\frac{1}{2}, \bar{y}, \frac{3}{4}\right)$, $6\left(\frac{1}{2}, \bar{y}, \frac{7}{4}\right)$, $7\left(\frac{3}{2}, \bar{y}, \frac{7}{4}\right)$, $8\left(\frac{3}{2}, 1-y, \frac{7}{4}\right)$.

independent combinations of spin components, P_y is expressed as the sum of nine terms:

$$\begin{aligned} P_y = {} & \delta_1(s_1^{a^2} + s_3^{a^2} - s_5^{a^2} - s_7^{a^2}) + \delta_2(s_1^{b^2} + s_3^{b^2} - s_5^{b^2} - s_7^{b^2}) + \delta_3(s_1^{c^2} + s_3^{c^2} - s_5^{c^2} - s_7^{c^2}) + \\ & + \delta_4(s_1^a s_1^c + s_3^a s_3^c - s_5^a s_5^c - s_7^a s_7^c) + \delta_5(s_1^b s_5^a - s_1^a s_5^b + s_3^b s_7^a - s_3^a s_7^b) + \delta_6(s_1^b s_5^c - s_1^c s_5^b + s_3^b s_7^c - s_3^c s_7^b) \\ & + \delta_7(s_1^b s_3^a - s_1^a s_3^b + s_5^b s_7^a - s_5^a s_7^b) + \delta_8(s_1^b s_3^c - s_1^c s_3^b + s_5^b s_7^c - s_5^c s_7^b) + \delta_9(s_3^a s_5^b - s_3^c s_5^a + s_1^c s_7^a - s_1^a s_7^c) \end{aligned} \tag{28}$$

in which the equilibrium relationships $\mathbf{s}_1 = \text{-}\mathbf{s}_2$, $\mathbf{s}_3 = \text{-}\mathbf{s}_4$, $\mathbf{s}_5 = \text{-}\mathbf{s}_6$ and $\mathbf{s}_7 = \text{-}\mathbf{s}_8$, which hold for all commensurate structures of $MnWO_4$, have been taken into account. The $\delta_1 - \delta_4$ terms in Eq. (28) are symmetric invariants involving a single atom. Their origin is entropic and due to on-site interactions. The $\delta_5 - \delta_9$ terms represent Dzialoshinskii-Moriya (DM) antisymmetric coupling interactions [24, 25] between neighbouring pairs of spins $\mathbf{s}_1$, $\mathbf{s}_5$ (or the equivalent pair $\mathbf{s}_3$, $\mathbf{s}_7$), $\mathbf{s}_1$, $\mathbf{s}_3$ ($\mathbf{s}_5$, $\mathbf{s}_7$) and $\mathbf{s}_3$, $\mathbf{s}_5$ ($\mathbf{s}_1$, $\mathbf{s}_7$). The DM interaction is currently assumed as the microscopic source of the polarization in the spiral structure of magnetic multiferroics. The preceding results on $MnWO_4$ confirm explicitly this view, but show that other symmetric effects are also involved in the formation of the electric dipoles. Furthermore, equilibrium relationships of the spin components in phase IV' and V' (Table 4) preserve the symmetric and DM contributions in Eq. (28). It indicates that the interactions giving rise to the polarization in the commensurate ferroelectric phases of multiferroic compounds are of the same nature than in the spiral phases. One should note that the DM interactions, as well as the Katsura-type contribution [26]

Table 4. Equilibrium values of the magnetic spins for phases I'-to-V' considered in the text.

Phase I`	$s_1^{a,c} = s_2^{a,c} = s_7^{a,c} = s_8^{a,c} = 0, s_3^b = s_4^b = s_5^b = s_6^b = 0,$ $s_3^{a,c} = -s_4^{a,c} = -s_5^{a,c} = s_6^{a,c}, s_1^b = -s_2^b = -s_7^b = s_8^b$
Phase II`	$s_1^{a,c} = -s_2^{a,c} = s_7^{a,c} = -s_8^{a,c} = -s_3^{a,c} = s_4^{a,c} = s_5^{a,c} = -s_6^{a,c}$ $s_1^b = -s_2^b = -s_7^b = s_8^b = s_3^b = -s_4^b = s_5^b = -s_6^b$
Phase III`	$s_1^{a,c} = -s_2^{a,c} = s_7^{a,c} - s_8^{a,c}, s_3^{a,c} = -s_4^{a,c} = -s_5^{a,c} = s_6^{a,c}$ $s_1^b = -s_2^b = s_7^b = -s_8^b, s_3^b = -s_4^b = s_5^b = -s_6^b$
Phase IV`	$s_1^b = s_5^b = 0, s_3^{a,c} = s_5^{a,c} = 0$ $\vec{s}_1 = -\vec{s}_2, \vec{s}_3 = -\vec{s}_4, \vec{s}_5 = -\vec{s}_6, \vec{s}_7 = -\vec{s}_8$
Phase V`	$s_3^b = s_5^b = 0, s_1^{a,c} = s_7^{a,c} = 0$ $\vec{s}_1 = -\vec{s}_2, \vec{s}_3 = -\vec{s}_4, \vec{s}_5 = -\vec{s}_6, \vec{s}_7 = -\vec{s}_8$

$\mathbf{e}_{ij} \times \mathbf{s}_i \times \mathbf{s}_j$ (where $\mathbf{e}_{ij}$ is the distance between neighbouring Mn atoms i and j), cancel in Eq. (28) when all spin components are cancelled except s_1^a and s_7^a in phase IV', or s_3^a and s_5^a in phase V', while keeping a finite value $P_y = \delta_1(s_1^{a^2} - s_7^{a^2})$ and $P_y = \delta_1(s_3^{a^2} - s_5^{a^2})$ in phases IV' and V'. Therefore symmetry considerations predict the existence of a polarization induced by symmetric interactions, although such effect may encounter considerable restrictions at the microscopic level.

4.3 Survey of the theoretical description of $RMnO_3$ and RMn_2O_5 multiferroics

A similar theoretical description than for $MnWO_4$ can be proposed for the sequence of three magnetic phases, denoted I-III, observed below $T_1 = 41$ K in $TbMnO_3$ [27–29], although the lower-temperature non-polar phase III arising below $T_3 = 7$ K is more complex than a simple lock-in structure of the ferroelectric spiral structure of phase II, stabilized below $T_2 = 28$ K. The similarity with $MnWO_4$ stems from the property that the two irreducible corepresentations involved in the phase sequence of $TbMnO_3$, denoted Δ_2 and Δ_3, have the *same image-group* than Γ^{k1} and Γ^{k2}, in spite of a different paramagnetic symmetry , and transition wave-vector $\vec{k} = (0, 0.28, 0)$. Therefore, the coupling of Δ_2 and Δ_3 yields for $TbMnO_3$ the same Landau expansion, given by Eq. (16), the same phase diagrams shown in Fig. 17, and an analogous hybrid "pseudo-proper" behaviour for the ferroelectric spiral phase. However, due to the higher *Pbnm*1' symmetry of the paramagnetic phase, the magnetic symmetries of the antiferromagnetic phases I an II display higher symmetric gray magnetic point groups, given in Fig. 22. Besides, the polarization-flop process in $TbMnO_3$ shows more complex features than in $MnWO_4$. Under applied magnetic field along the x or y directions, the spontaneous P_z polarization existing at zero field in the spiral phase of $TbMnO_3$ is switched along the x direction above threshold fields $B_x^{th} \approx 9$ T and $B_y^{th} \approx 4.5$ T, respectively, at a first-order lock-in transition to a commensurate phase with $\vec{k} = (0, \frac{1}{4}, 0)$. The first-order transition process can be decomposed in two stages: Under B_x or B_y field the spiral phase II is switched to a lower symmetric ferroelectric phase, above threshold fields given by the stability condition of phase II under B_x or B_y field, which triggers a *decoupling* of the two order-parameters involved in phase II, and a lock-in transition to a ferroelectric phase, associated with a single order-parameter. This phase has the symmetry 2*mm,* which cancels P_z and gives rise to P_x. Such interpretation

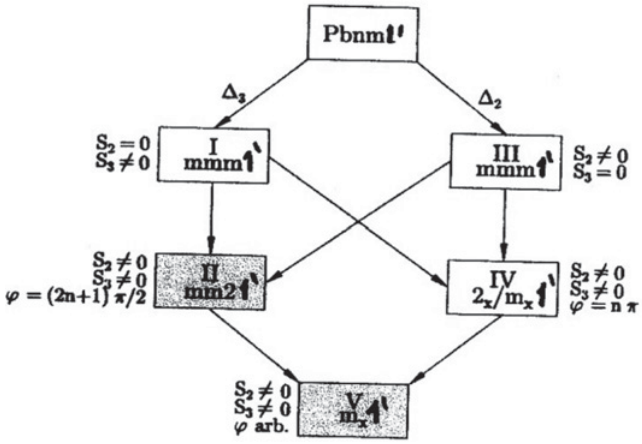

Figure 22. Connections between the magnetic point-groups I-V and corresponding equilibrium conditions fulfilled by the order-parameters inducing the sequence of phases observed in $TbMnO_3$.

in terms of a two-stage process is supported by the observation in $TbMnO_3$ of the coexistence of distinct structural phases in the intermediate field regime [30]. Another support is provided by the observation in $DyMnO_3$ of similar field-induced flops [31], not associated with a high-field commensurate lock-in phase. It implies the stabilization of an intermediate phase with 2_x symmetry induced by magnetoelectric couplings $\kappa_1 P_x M_x M_z S_2 S_3 \sin\varphi$ or $\kappa_2 P_x M_x M_y S_2 S_3 \sin\varphi$ under B_x or B_y fields, where $\bar{S}_2$ and $\bar{S}_3$ are the order-parameters transforming as Δ_2 and Δ_3.

A different situation is found in $TbMn_2O_5$ [32] due to the property that a single four-dimensional irreducible corepresentation induces the spiral phase observed in this compound. On cooling below the paramagnetic (P) phase, of symmetry *Pbam*1', $TbMn_2O_5$ undergoes five phase transitions taking place successively at $T_1 = 43\,\mathrm{K}$, $T_2 = 38\,\mathrm{K}$, $T_3 = 33\,\mathrm{K}$, $T_4 = 24\,\mathrm{K}$ and $T_5 = 10\,\mathrm{K}$ [33, 34], the corresponding phases being denoted I-V. The $\mathrm{P} \rightarrow \mathrm{I} \rightarrow \mathrm{II}$ sequence of incommensurate phases is associated with a four-component order-parameter transforming as an irreducible corepresentation, denoted G_1, with the wave-vector $\vec{k} = (1/2, 0, k_z)$ At $T_3 = 33\,\mathrm{K}$ the commensurate phase III takes place for $\vec{k} = (1/2, 0, 1/4)$ preserving the dimensionality, but not the symmetry of the order-parameter. By contrast the incommensurate phases IV and V correspond to the coupling of two four-dimensional order-parameters associated with two irreducible corepresentations, denoted Ξ_1 and Ξ_2, at $\vec{k} = (0.48, 0, 0.32)$.

The four-component order-parameter associated with the $\mathrm{P} \rightarrow \mathrm{I} \rightarrow \mathrm{II}$ transitions can be denoted $S_1 = \rho_1 e^{i\theta_1}$, $S_1^* = \rho_1 e^{-i\theta_1}$, $S_2 = \rho_2 e^{i\theta_2}$ and $S_2^* = \rho_2 e^{-i\theta_2}$. It yields the invariants $\Im_1 = \rho_1^2 + \rho_2^2$, $\Im_2 = \rho_1^2\rho_2^2$ and $\Im_3 = \rho_1^2\rho_2^2 \cos 2\theta$, with $\theta = \theta_1 - \theta_2$, and the Landau expansion:

$$\Phi_1(\rho_1, \rho_2, \theta) = a_1\Im_1 + a_2\Im_1^2 + b_1\Im_2 + b_2\Im_2^2 + c_1\Im_3 + c_2\Im_3^2 + d\Im_1\Im_3 + \ldots \tag{29}$$

Minimizing Φ_1 shows that seven phases can be stabilized below the P phase for different equilibrium values of ρ_1, ρ_2 and θ, summarized in Fig. 23. The corresponding phase diagrams in the orbit space $(\Im_1, \Im_2, \Im_3)$ and in the coefficient spaces (a_1, b_1, c_1) and (b_1, c_1), are shown in Fig. 24. Phases I and II of $TbMn_2O_5$ correspond to phases 1 ($\rho_1 \neq 0, \rho_2 = 0$) and 6 ($\rho_1 \neq \rho_2, \theta = (2n+1)\pi/2$) in Fig. 23, which display the magnetic point-groups *mmm*1' and *m*2*m*. The equilibrium polarization in phase II, deduced from the dielectric free-energy

$$\Phi_1^D = \delta_1\rho_1\rho_2 P_y \sin\theta + \frac{P_y^2}{2\varepsilon_{yy}^0}, \text{ is}$$

$$P_y^e = \pm\delta_1\varepsilon_{yy}^0\rho_1\rho_2 \tag{30}$$

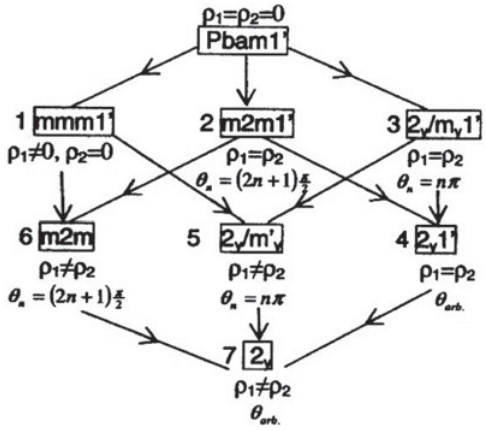

Figure 23. Connections between the magnetic point-groups of phases 1-7 induced by the irreducible corepresentation, denoted G_1 in ref. [32], of the $Pbam1'$ paramagnetic structure of $TbMn_2O_5$, and equilibrium conditions fulfilled by the order-parameter in each phase.

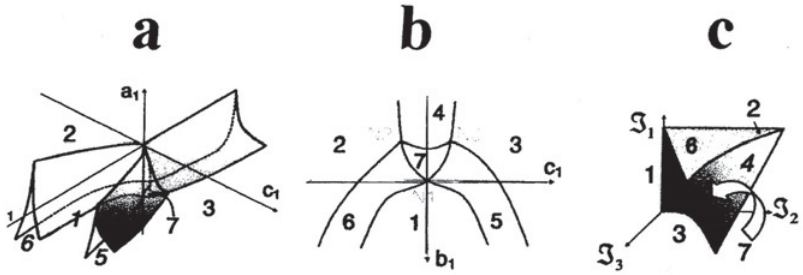

Figure 24. Phase diagrams deduced from the minimization of the Landau expansion given by Eq. (29) in **(a)** the (a_1, b_1, c_1) space, **(b)** the (b_1, c_1) plane for $a_1 < 0$, and **(c)** the orbit space $(\Im_1, \Im_2, \Im_3)$.

corresponding to an effective *linear* dependence of P_y^e on ρ_2, since ρ_1 has been already activated in phase I. Therefore, below T_2, in the ferroelectric phase II, one has $P_y^e(T) \propto (T_2 - T)^{1/2}$ (Fig. 25(a)), and the same temperature dependence, given by Eq. (20), for the dielectric permittivity $\varepsilon_{yy}(T)$ (Fig. 25(b)). Therefore the transition to phase II shows the same hybrid behaviour as the analogous transitions in $TbMnO_3$ and $MnWO_4$, i.e. it behaves critically as a proper ferroelectric transition, although the value of the polarization (about $40\,nC/cm^2$) in phase II is that of an improper ferroelectric.

At $T_3 = 33\,K$ the wave-vector locks into the commensurate value $\vec{k} = (1/2, 0, 1/4)$ giving rise to the (umklapp) invariants $\rho_1^4 \cos 4\theta_1 + \rho_2^4 \cos 4\theta_2$ and $\rho_1^2 \rho_2^2 \cos 2(\theta_1 + \theta_2)$. The symmetry of the order-parameter is changed but not its dimensionality. Taking into account these additional invariants yields an equilibrium ferroelectric phase for $\theta_1 = \pm\theta_2 = n\pi/4$, having the same magnetic point-group symmetry $m2m$ as phase II, with a commensurate lattice parameter 4c. The transition coincides with a slight change in the slope of $P_y^e(T)$ (Fig. 25(a)), and no noticeable anomaly of the dielectric permittivity. In contrast the transition occurring at $T_4 = 24K$ to phase IV exhibits a finite jump of $\varepsilon_{yy}^e(T)$ which reflects a typical improper ferroelectric transition. The improper character of the transition is consistent with the form of the polarization in phase IV which is:

$$P_y^e = \pm\delta_2 \varepsilon_{yy}^0 \rho_1 \rho_3 \tag{31}$$

where ρ_1 and ρ_3, which are amplitudes of two distinct four-dimensional order-parameters which are both activated at the III $\rightarrow$ IV transition mechanism, vary as $\propto (T_4 - T)^{1/2}$ for $T < T_4$. Therefore, P_y

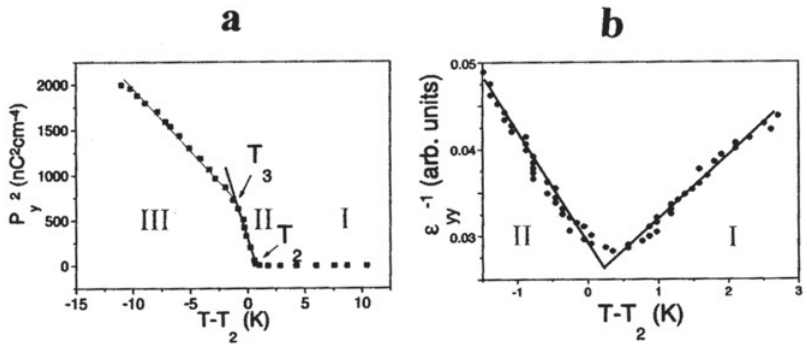

Figure 25. Least square fits for **(a)** the squared polarization $P_y^{e2} \propto (T_2 - T)$ and **(b)** the inverse dielectric permittivity $\varepsilon_{yy}^{-1} \propto |(T_2 - T)|$ reported by Hur et al [33].

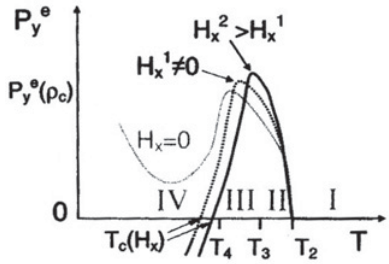

Figure 26. Temperature dependence of $P_y^e(T, H_x)$ given by Eq. (34) for $\delta_1 > 0, \delta_2 < 0, \nu < 0$.

varies linearly as $(T_4 - T)$, which expresses a typical improper ferroelectric behaviour for the III $\rightarrow$ IV transition. The dielectric permittivity below T_4 is given by $\varepsilon_{yy}^e(T_4) = \frac{\varepsilon_{yy}^0}{1-\delta_2^2 \varepsilon_{yy}^0 f}$, where $0 < f < 1$ represents a combination of phenomenological coefficients.

Below T_4, $P_y^e(T)$ is the sum of two distinct contributions given by Eqs. (30) and (31):

$$P_y^e(T) = \pm\varepsilon_{yy}^0 \left[\delta_1 \rho_1 (T_2 - T)^{1/2} + \delta_2 (T_4 - T)\right] \tag{32}$$

where $\rho_1 \propto (T_1 - T_2)^{1/2}$. Assuming $\delta_1 > 0$ and $\delta_2 < 0$, one can verify that $P_y^e(T)$ decreases for $T \leq T_{Max} = T_2 - \frac{\delta_1^2}{4\delta_2^2}(T_1 - T_2)$ The strong increase observed below T_5 reflects a positive contribution to the total polarization of the electric polarization in phase V (Fig. 26). Under applied magnetic field H_x the spontaneous polarization in phase IV becomes:

$$P_y^e(H_x) = \pm\varepsilon_{yy}^0 \rho_1 \rho_3 (\delta_2 + \nu \mu_0^{-2} H_x^2) \tag{33}$$

due to the magnetoelectric coupling $\nu \rho_1 \rho_3 P_Y M_x^2$. For $\nu < 0$ the application of a H_x field enhances the negative contribution to the temperature dependence of the total polarization, leading to:

$$P_y^e(T, H_x) = \pm\varepsilon_{yy}^0 \left[\delta_1 (T_1 - T_2)^{1/2} (T_2 - T)^{1/2} + (\delta_2 + \nu \mu_0^{-2} H_x^2)(T_4 - T)\right] \tag{34}$$

Therefore, $P_y^e(T, H_x)$ changes sign for the temperature dependent threshold field

$$H_x^c(T)^2 = -\frac{\mu_0^2}{\nu}\left[\delta_2 + \frac{\delta_1 (T_1 - T_2)^{1/2} (T_2 - T)^{1/2}}{(T_4 - T)}\right] \tag{35}$$

as shown in Fig. 26.

Similar sequences of ferroelectric phases are found in other RMn_2O_5 compounds [35–37], where R = Bi, Y or a rare-earth heavier than Nd. In these compounds, at variance with $TbMn_2O_5$ in which the pseudo-proper coupling occurs between *distinct components of the same order-parameter,* the pseudo-proper coupling is created between two distinct four-component order-parameters associated with the wave-vector $\vec{k} = (k_x, 0, k_z)$. However, with the exception of $DyMn_2O_5$ and $BiMn_2O_5$, the order-parameters involved in the RMn_2O_5 family correspond to the symmetries disclosed for R = Tb, i.e., to $\vec{k} = (1/2, 0, k_z), (k_x, 0, k_z)$ and $(1/2, 0, 1/4)$.

5. PHASE TRANSITIONS INDUCED BY REPLICA OF THE SAME ORDER-PARAMETER: UNCONVENTIONAL STATES OF SUPERCONDUCTORS AND LIQUID CRYSTALS

5.1 Specific property of phase transitions associated with continuous symmetry groups

In the preceding sections the parent structure was described by a *discrete,* crystallographic or magnetic, symmetry group. When *continuous* groups are involved, the lowest symmetry group induced by an irreducible representation Γ of dimension $n \geq 2$ of the parent symmetry group G_0, can only be obtained by considering the reducible representation $\Gamma + \Gamma + \Gamma + ...$, the number of $\Gamma's$ figuring in the sum being smaller or equal to n. This result stems from the specific property of continuous groups that the minimal symmetry group G_m induced by Γ (defined as the invariance group of the general direction in the representation space) does not coincide with the lowest symmetry group G_k associated with Γ (corresponding to the kernel of the homomorphism of G_0 on $\Gamma(G_0)$). Therefore, in order to obtain the full set of broken symmetry phases associated with a given irreducible representation Γ of a continuous group, one has to consider different *replica* of Γ. We will illustrate this property by considering examples of phase transitions in superconducting and liquid crystal systems, which are both described by continuous symmetry groups.

5.2 Unconventional s-pairing wave superconductivity

The parent (Normal) state of a superconductor is generated by four groups:

$$G_0 = [U(1) \times T] \otimes O_R(3) \otimes O_S(3) \tag{36}$$

Where $U(1)$ is the continuous group generated by gauge operations g_α. T is the group formed by the time-reversal operation T and the identity. O_R (3)and O_S (3) are, respectively, the full orthogonal group in real and spin spaces. In the Ginzburg-Landau theory of superconductivity [5], the transition to the superconducting state is associated with a two-component s-pairing wave order-parameter corresponding to a complex wave function $\Psi_1 = \rho_1 e^{i\theta_1}$ and its complex conjugate $\Psi_1^* = \rho_1 e^{-i\theta_1}$. It transforms as a two-dimensional irreducible representation Γ of G_0 which can be written:

$$\Gamma = \tau_1 \times V \tag{37}$$

where τ_1 is the identity irreducible representation of O_R (3) $\otimes O_S$ (3) and V is the vector representation of U (1) $\times T$. The single superconducting state induced by Γ has the same structural symmetry as the normal state and is time-reversal invariant: Only the gauge-symmetry is broken at the Normal-to-superconducting transition. Let us show that the phase diagram associated with the four-component reducible order-parameter $(\Psi_1, \Psi_1^*, \Psi_2 = \rho_2 e^{i\theta_2}, \Psi_2^* = \rho_2 e^{-i\theta_2})$ transforming as $\Gamma + \Gamma$ contains *two different superconducting states,* which possess respectively the *minimal symmetry* G_m and the *lowest symmetry* G_k associated with Γ [38]. From the transformation properties of the order-parameter components under the symmetry operations of G_0 one finds for any continuous or discrete symmetries of O_R (3) $\times O_S$ (3), the following invariant monomials: $\Im_1 = \rho_1^2$, $\Im_2 = \rho_2^2$ and $\Im_3 = \rho_1 \rho_2 \cos(\theta_1 - \theta_2)$, which give the Landau expansion:

$$\Phi(\rho_i, \theta_i) = a_1\Im_1 + a_2\Im_1^2 + b_1\Im_2 + b_2\Im_2^2 + c_1\Im_3 + c_2\Im_3^2 + d_1\Im_1\Im_2 + d_2\Im_1\Im_3 + d_3\Im_2\Im_3 + \ldots . \tag{38}$$

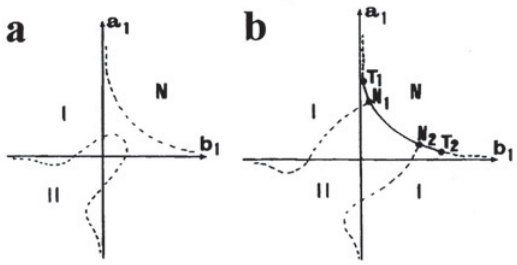

Figure 27. Phase diagrams in the (a_1, b_1) plane, corresponding to the Landau expansion given by Eq. (38), and truncated either at the fourth degree ((**a**)), or at the sixth degree ((**b**)). Dashed and full lines are, respectively, second-order and first-order transition lines. N_1 and N_2 are three-phase points; T_1 and T_2 are tricritical points.

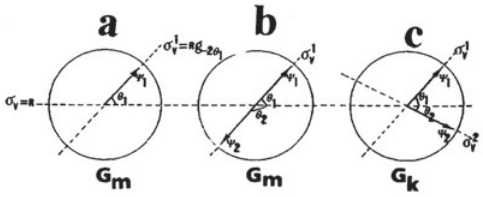

Figure 28. Difference between the minimal (G_m) and lowest (G_k) symmetry groups describing the superconducting states associated with the Γ representation defined by Eq. (37). The order-parameters Ψ_1 and Ψ_2, transforming as Γ, are represented in the complex plane schematized by a circle. The gauge (g_α) and time-reversal (T) operations act as rotations and reflections (σ_v) in this plane. When only one (**a**) or two collinear order-parameters (**b**) are involved a single superconducting state (I) is stabilized, which possesses the minimal symmetry **Gm** generated by the reflection $\sigma_v^1 = T g_{-2\theta_1}$. At variance, when Ψ_1 and Ψ_2 are dephased (**c**) and additional superconducting state (II) can be stabilized, which possesses the lowest symmetry group **Gk** reduced to the identity: the time reversal symmetry T is lost.

Minimization of Φ yields three possible stable states, which are represented in the phase diagrams of Fig. 27. In addition to the Normal state of symmetry G_0, which is stable for $\rho_1 = \rho_2 = 0$, two different superconducting states can be stabilized:

1) State I, corresponding to $(\rho_1 \neq 0, \rho_2 = 0)$ or $(\rho_1 = 0, \rho_2 \neq 0)$ or $(\rho_1 \neq 0, \rho_2 \neq 0, \theta_1 - \theta_2 = 0, \pi)$. It has the minimal symmetry group G_m of the conventional s-pairing superconducting state, namely $G_m = [O_R(3) \otimes O_S(3)] \times H_m$, where H_m is generated by the symmetry operation $\mathrm{T}.g_{-2\theta_1}$ in which time reversal symmetry combines with the gauge symmetry (Figs. 28(a) and (b)). As shown in Fig. 27(a), state I can be reached from the Normal phase across a second-order transition.

2) State II, which is stabilized for $\rho_1 \neq 0, \rho_2 \neq 0$ and $\theta_1 - \theta_2 \neq 0, \pi$. It has the lowest symmetry $G_k = O_R(3) \otimes O_S(3)$ associated with the irreducible representation Γ (Fig. 28(c)). Accordingly, at the Normal→State II and State I →State II transitions, *the time reversal symmetry is broken even when assuming an isotropic symmetry in real and spin spaces.* The spontaneous physical quantity arising in phase II transforms as:

$$\eta = \frac{i}{2}(\Psi_1 \Psi_2^* - \Psi_1^* \Psi_2) = \rho_1 \rho_2 \sin(\theta_1 - \theta_2) \tag{39}$$

A non vanishing macroscopic physical quantity corresponding to η is $(\vec{E}_1 \times \vec{E}_2).\vec{H}$, where $\vec{E}_1$ and $\vec{E}_2$ are differently oriented electric fields, and $\vec{H}$ is a magnetic field. In this case η identifies to a combination of components of the third-rank tensor α_{ijk} characterizing a *second-order magnetoelectric effect* expressed by:

$$\vec{P} = \varepsilon \vec{E} + \eta(\vec{E} \times \vec{H}) \tag{40}$$

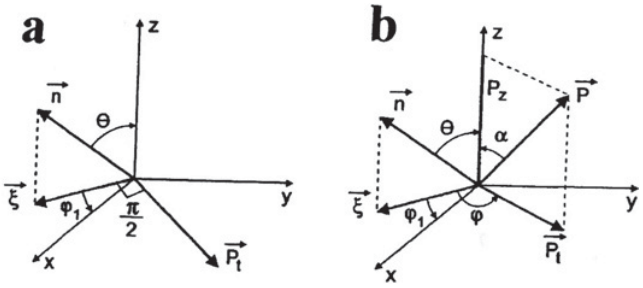

Figure 29. In-plane configurations of (**a**) the Sm-C^* phase, and (**b**) the Sm-C^*_P phase.

where $\vec{P}$ is the polarization induced by the conjuncted application of $\vec{E}$ and $\vec{H}$, and ε is the dielectric permittivity. Note that $\vec{P}$ will appear perpendicularly to $\vec{E}$ under application of $\vec{H}$. Note also that the reciprocal magnetoelectric effect, corresponding to the equation of state $M_i = \alpha_{ijk} E_j E_k$ will not be observable, since the induced magnetization vanishes identically.

5.3 Unconventional chiral ferroelectric liquid crystal phase

A close analogy with the s-pairing wave superconducting states can be found in the ferroelectric phases of chiral liquid crystals formed from rod-like molecules [39, 40]. The order-parameter of the $Sm-A* \rightarrow Sm-C*$ phase transition is a two-component tilt vector $\vec{\xi} = (\xi_1, \xi_2)$ describing the magnitude and the tilt of the long molecular axis $\vec{n}$ from the normal $\vec{z}$ to the smectic layers, with a tilt angle θ. Because of the chirality of the molecules, a linear coupling between the tilt and the in-plane polarization exists, leading to a spontaneous transverse polarization $\vec{P}_t = (P_x, P_y)$ perpendicular to $\vec{n}$ and $\vec{\xi}$ (Fig. 29(a)). The precession of $\vec{n}$ around the $\vec{z}$ direction, results in a helical ferroelectric $Sm-C*$ phase, having a zero spontaneous macroscopic polarization. Considering a bilinear coupling between the components of $\vec{\xi}$ and $\vec{P}_t$ implies assuming a four-component *reducible* order-parameter $\Psi = (\xi_1, \xi_2, P_x, P_y)$ which transforms as the sum $\mathrm{E}_1 + \mathrm{E}_2$ of two *identical* irreducible representations associated with the D_∞ symmetry-group of the $Sm-A*$ phase. In this case the monoclinic C_2 symmetry of the $Sm-C*$ phase, which corresponds to orthogonal directions for $\vec{\xi}$ and $\vec{P}_t$, is not the lowest symmetry involved by the $\mathrm{E}_1 + \mathrm{E}_2$ representation. The lowest symmetry is triclinic C_1, and coincides with an angle $\varphi \neq \pi/2$, between $\vec{\xi}$ and $\vec{P}_t$. Let us show that the corresponding triclinic smectic configuration, which displays a spontaneous polarization component P_z (Fig. 29(b)), can be stable.

From the transformation property of the four-component order-parameter Ψ under the symmetry operations of D_∞ one finds the following independent invariants $\Im_1 = \xi_1^2 + \xi_2^2 = \xi^2, \Im_2 = P_x^2 + P_y^2 = P_t^2$ and the piezoelectric coupling invariants $\Im_3 = \xi_1 P_y - \xi_2 P_x = \xi P_t \sin\varphi$ and $\Im_4 = P_z(\xi_1 P_x + \xi_2 P_y) = P_z \xi P_t \cos\varphi$. The corresponding Landau free-energy density reads:

$$\Phi(\xi, P_t, \varphi, P_z) = a_1\xi^2 + a_2\xi^4 + \frac{P_t^2}{2\varepsilon^0_{xx}} + b_1 P_t^4 - c_1 \xi P_t \sin\varphi + c_2 \xi^2 P_t^2 \sin^2\varphi - d_1 P_z \xi P_t \cos\varphi + \frac{P_z^2}{2\varepsilon^0_{zz}} \tag{41}$$

Minimization of Φ shows that, in addition to the parent $Sm-A*$ phase ($\xi^e = P_t^e = 0$), two distinct tilted smectic configurations with $\xi \neq 0$ and $P_t \neq 0$ can be stabilised: 1) The standard $Sm-C*$ configuration shown in Fig. 29(a), for $\varphi^e = (2n+1)\pi/2$, which has the monoclinic C_2 symmetry, and the spontaneous polarization $P_t^e = c_1 \varepsilon^0_{xx} \xi$, denoting the *pseudo-proper* character of the ferroelectric order in liquid crystals. 2) The $Sm-C^*_P$ configuration, shown in Fig. 29(b), which is stabilized for $\sin\varphi^e = \frac{c_1}{P_t^e \xi^e (2c_2 - d_1^2 \varepsilon^0_{zz})} \neq 0, \pm\pi/2, \pi$. It has the symmetry C_1 and a spontaneous polarization in general direction, with a P_z component given by $P_z^e = d_1 \varepsilon^0_{xx} \xi^e P_t^e \cos\varphi^e$. Note that P_z^e results from a

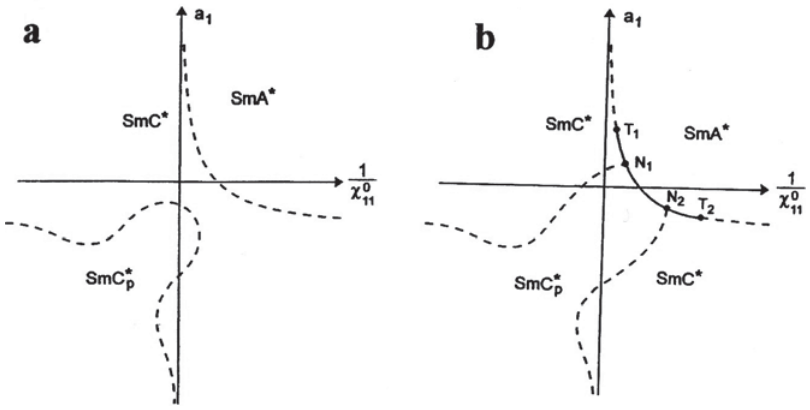

Figure 30. Phase diagrams corresponding to the Landau expansion Φ defined by Eq. (41), assuming (**a**) a fourth degree expansion in ξ and P_t, (**b**) a sixth degree expansion.

second-order piezoelectric effect, i.e. from the simultaneous existence of tilt-angle and in-layer polarization, under the condition that the scalar product $\vec{\xi}.\vec{P}_t \neq 0$. The phase diagrams involving the $Sm-C*$ and $Sm-C_P^*$ phases are shown in Fig. 30. They are topologically identical to the phase diagrams of Fig. 27.

6. RECONSTRUCTIVE PHASE TRANSITIONS

6.1 Phase transitions between group-subgroup unrelated structures

Continuous or slightly discontinuous structural transitions have been the almost exclusive subject of the theoretical approaches to phase transitions: From the initial work of Landau (in which the author assumes a group-subgroup relationship between the symmetries of the phases) to the different statistical physics approaches, such as the Ising model (which leads to a lowering of symmetry with respect to the initial structure), and the sophisticated theory of critical phenomena. However, the most widespread and fundamental types of structural transitions found in nature involve no group-subgroup relationship between the phase symmetries. In this respect, two different situations should be distinguished. The phases may correspond to different equilibrium components of the same order-parameter and display different subgroups of a common parent symmetry group. This is, for example, the case of the low temperature phases of Barium titanate, corresponding to subgroups of the $Pm\bar{3}m$ perovskite symmetry. Here, the structures of the phases are closely related between them by small structural modifications, across slightly discontinuous transitions. *Reconstructive phase transitions* [3, 41–44] belong to another class in which the transition mechanisms exhibit drastic changes, with critical displacements of the order of magnitude of the lattice parameters, large latent heat and thermal hysteresis, and an eventual breaking of part of the chemical bonds. In the following subsections we show that despite the preceding features, a theoretical description of reconstructive transitions can be performed, preserving the main concepts of the Landau approach.

6.2 Basic ideas of the theory of reconstructive transitions

We summarize hereafter the basic ideas of the theory of reconstructive phase transitions, assuming that the transition mechanism can be formulated in terms of atomic displacements. Let us consider two phases A and B having no group-subgroup relationship between the space-groups G_A and G_B describing their structures. G_A and G_B possess common subgroups G_1, G_2, G_3 . . ..corresponding to common stable

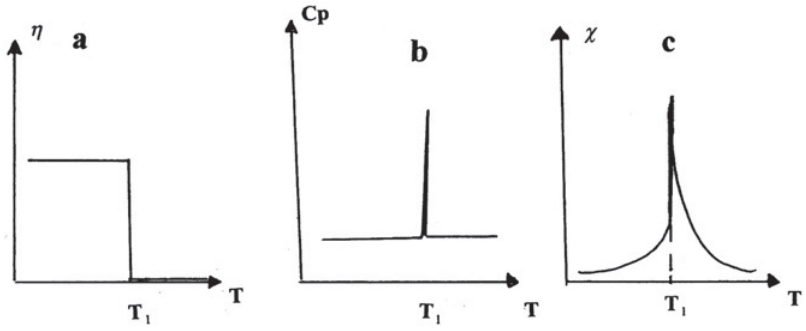

Figure 31. (a) Step-like dependence on temperature for the order-parameter associated with a reconstructive transition. Temperature dependence of the specific heat (**b**) and susceptibility (**c**) for a reconstructive transition.

substructures of the A and B structures. Starting from the A structure, the reconstructive mechanism transforming A in B proceeds via a critical displacement field ξ_i going across one of the substructures of A and B associated with one of the G_i subgroups denoted G_{AB}, which fulfils the following constraints: 1) It corresponds to the set of *minimal* critical displacements permitting to reach the B structure. 2) It is compatible with the observed epitaxial relationships between A and B and with the various experimental data reported for the two phases (domains, strains, vibration spectra...).

3) It is consistent with the transition mechanisms leading to other stable phases having regions of stability in the phase diagram. Accordingly, the determination of the transition path transforming A into B cannot be simply based on symmetry (group-theoretical) considerations but requires a careful analysis of the real structures, and of the available experimental observations on the transition.

For vanishingly small or non specific critical displacements, the symmetry of the initial A structure is lowered to G_{AB}. The B structure is obtained for *specific large fractional displacements* ξ_i at which the *new symmetry elements* pertaining to the B structure arise. Furthermore, determining the order-parameter symmetry from the irreducible representations Γ_1 and Γ_2 associated, respectively, with the hypothetical $G_A \rightarrow G_{AB}$ and $G_B \rightarrow G_{AB}$ transitions, one can show that the order-parameter modulus η of the $G_A \rightarrow G_B$ reconstructive transition *is a periodic function* $\eta(\xi_i)$ *of the critical displacements*, whose minima and maxima coincide with G_B, whereas $\eta(\xi_i) = 0$ corresponds to G_A. Therefore, the Landau expansion $\Phi(\eta(\xi_i))$ has to be minimized with respect to the ξ_i variables, the equations of state $\frac{\partial \Phi}{\partial \xi_i} = \frac{\partial \Phi}{\partial \eta} \cdot \frac{\partial \eta}{\xi_i} = 0$ showing that two types of equilibrium states can be distinguished: 1) *Landau states* obtained for $\frac{\partial \Phi}{\partial \eta} = 0$, which are group-subgroup related to the A and B structures; 2) *Limit (non-Landau)* states, given by $\frac{\partial \eta}{\partial \xi_i} = 0$, for which the group-subgroup relationship is lost. As a consequence of the periodic-dependence on the critical displacements of the order-parameter, the order-parameter space becomes a *fibre bundle* instead of a Hilbert space for group-subgroup related transitions. Another consequence is the specific critical properties of reconstructive phase transitions, such as i) the step-like temperature dependence of the order-parameter, since the initial and final structures correspond to fixed displacements (Fig. 31(a)); ii) the delta-shaped specific heat at the transition (Fig. 31(b)), and iii) the finite discontinuity of the susceptibility associated with the field-conjugate to the order-parameter (Fig. 31(c)). Besides, since symmetry operations are lost at both the A → B and B → A transitions, domains are formed in both phases, in contrast to group-subgroup related phases where domains are observed only in the "daughter" phase.

6.3 The graphite-diamond reconstructive transition

As a first illustrative example let us consider the reconstructive transition mechanism between the graphite and diamond structures [45, 46]. Figure 32 represents the assumed displacive mechanisms

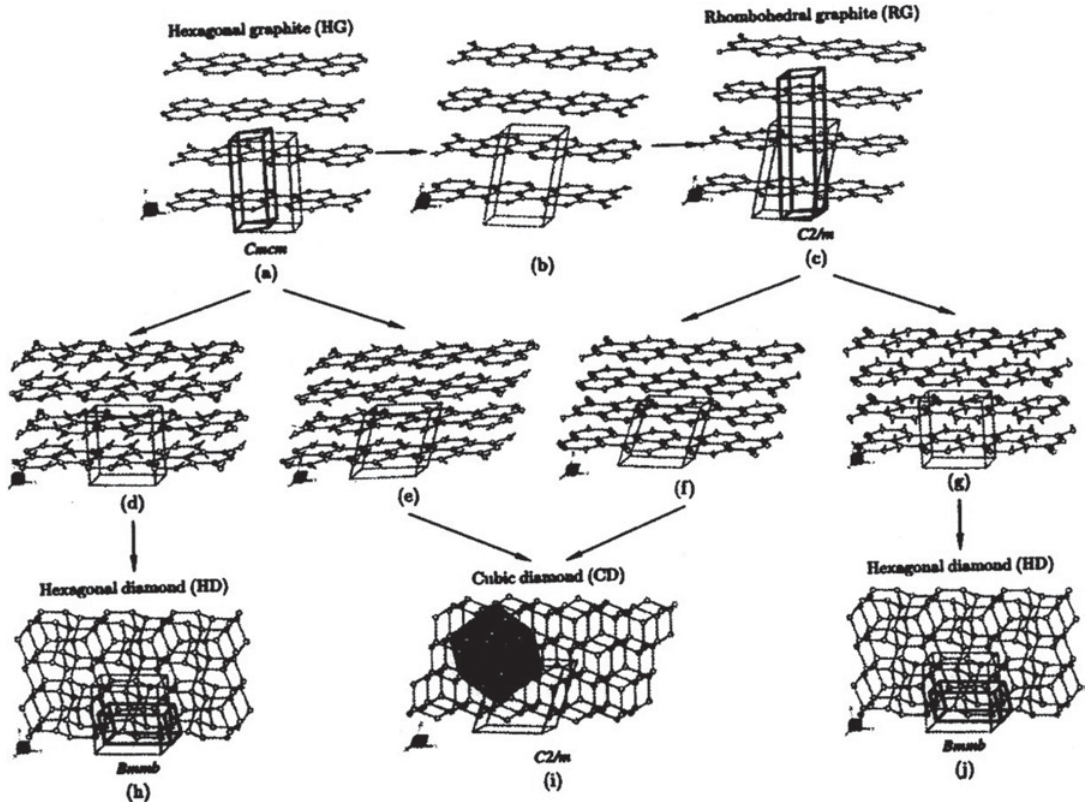

Figure 32. Structural mechanisms for the reconstructive phase transitions between carbon polymorphs via a common substructure. The conventional hexagonal and cubic unit-cells are represented by thick lines. The unit-cells of their common substructures are shown by thin lines. The small arrows represent the real magnitudes of the atomic displacements.

transforming hexagonal graphite (HG) ($P6_3/mmc$, Z = 4), rhombohedral graphite (RG) ($R\bar{3}m$, Z = 6), hexagonal diamond (HD) ($P6_3/mmc$, Z = 4) and cubic diamond (CB) ($Fd\bar{3}m$, Z = 8) into each other. The figure shows that the different carbon structures possess a common substructure displaying an orthorhombic *Cmcm* (HG), *Bmmb* (HD, or monoclinic $C2/m$ (RG, CD) symmetry, whose basic vectors $(\vec{a}, \vec{b}, \vec{c})$ are related with the basic vectors of the conventional hexagonal (HG, RG, HD) or cubic (CD) unit cells of the different allotropes by:

$$\begin{aligned}
\vec{a} &= \vec{a}_{HG} = \vec{a}_{RG} = -\vec{a}_{HD} = \tfrac{1}{2}(\vec{a} + \vec{b})_{CD} \\
\vec{b} &= (\vec{a} + 2\vec{b})_{HG} = (\vec{a} + 2\vec{b})_{RG} = \vec{c}_{HD} = -\tfrac{1}{2}(\vec{a} + \vec{b} - 2\vec{c})_{CD} \\
\vec{c} &= \vec{c}_{HG} = \tfrac{1}{3}(\vec{a} + 2\vec{b} + 2\vec{c})_{RG} = (\vec{a} + 2\vec{b})_{HD} = \tfrac{1}{2}(\vec{a} + \vec{b} + 2\vec{c})_{CD}
\end{aligned} \tag{42}$$

In agreement with the observed orientational relationships $[001]_{HG}//[120]_{HD}$, $[100]_{HG}//[100]_{HD}$ and $[120]_{HG}//[001]_{HD}$, the atomic displacements transforming HG into HD is shown in Figs. 32(a) → (d) → (h). It consists of antiparallel fractional displacements $\pm\frac{1}{16}\vec{b}$ and $\pm\frac{1}{12}\vec{c}$ combined with $\pm\frac{5}{48}\vec{b}$ and $\pm\frac{1}{12}\vec{c}$. The HG → HD transition involves a drastic compression of about 35% along $\vec{c}$ and small decompression (2%) and compression (6%) along $\vec{a}$ and $\vec{b}$, respectively. A similar mechanism, represented in Figs. 32(a) → (e) → (i), holds for the HG → CD transition. Starting from the transformed uni-cell of HG, the CD structure results from a reduction of the angle α from 90° in HG

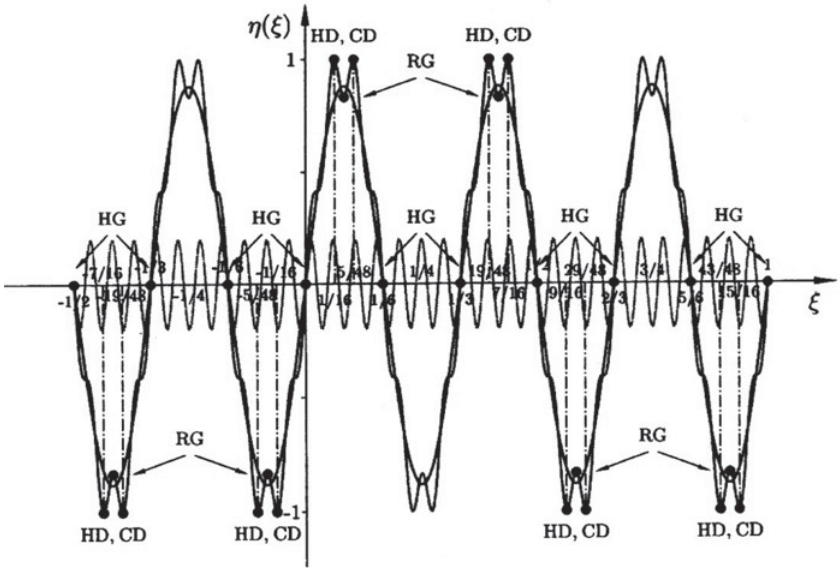

Figure 33. Periodic dependence (dark grey curve) of the effective transition order-parameter $\eta(\xi)$, defined by Eq. (43), associated with the transition from hexagonal graphite (HG) to rhombohedral graphite (RG), cubic diamond (CD) and hexagonal diamond (HD), in function of the critical displacements along $[120]_{HG}$.The curve in black represents the periodicity of the displacements giving rise to the RG structure (first term in Eq. (43)). The light-grey curve is a higher harmonic (second term in Eq. (43)) whose periodicity reflects the onset of the HD and CD structures from HG and RG, respectively.

to 70.529° in CD, and a set of antiparallel fractional displacements: $\pm\frac{1}{16}\vec{b}$ and $\pm\frac{1}{16}\vec{c}$, combined with $\pm\frac{5}{48}\vec{b}$ and $\pm\frac{1}{16}\vec{c}$. The transition involves a large compression of 35% along $\vec{c}$ and small decompressions (2%) along $\vec{a}$ and $\vec{b}$. The HG→RG transition mechanism shown in Figs. 32(a) → (b) → (c), consists of a reduction of the angle α from 90° in HG to 78.040° in RG, and of fractional displacements of the carbon atoms by $\pm\frac{1}{12}\vec{b}$.

The order-parameters associated with the transitions from HG to the other carbon polymorphs are of two types. (1) Macroscopic strains which consist of (i) the shear strain e_{yz} expressing the changes in the angle α and reduces the hexagonal HG symmetry to monoclinic, (ii) the tensile strain e_{xx}-e_{yy} corresponding to an orthorhombic deformation of the hexagonal cell, (iii) the compression e_{zz} along $\vec{c}$. (2) A cooperative set of fractional displacements along $\vec{b}$ and $\vec{c}$. Both types of order-parameters are activated for obtaining the polymorphic structures, which appear as limit states, arising for definite atomic displacements and critical strains. The periodic character of the reconstructive transition mechanisms is illustrated in Fig. 33, in which the order-parameter is plotted as a function of the atomic displacements ξ along the [120] direction in HG. The periodic function $\eta(\xi)$ representing the effective order-parameter associated with the HG →(HD, CD, RG) transitions is the truncated Fourier series:

$$\eta(\xi) = 0.958\sin(6\pi\xi) + 0.125\sin(42\pi\xi) \tag{43}$$

The first term in Eq. (43) expresses the "primary" symmetry-breaking displacements giving rise to the RG structure from HG, and the second term is a higher harmonic related to secondary displacements leading to the HD and CD structures from HG and RG, respectively. Taking into account the transformation properties of the displacements ξ by the symmetry operations of the HG space-group, yields two distinct effective free-energies $F_1(\eta(\xi)) = \frac{\alpha}{2}\eta^2 + \frac{\beta}{4}\eta^4 + \frac{\gamma}{6}\eta^6$, for the HG →(RG,

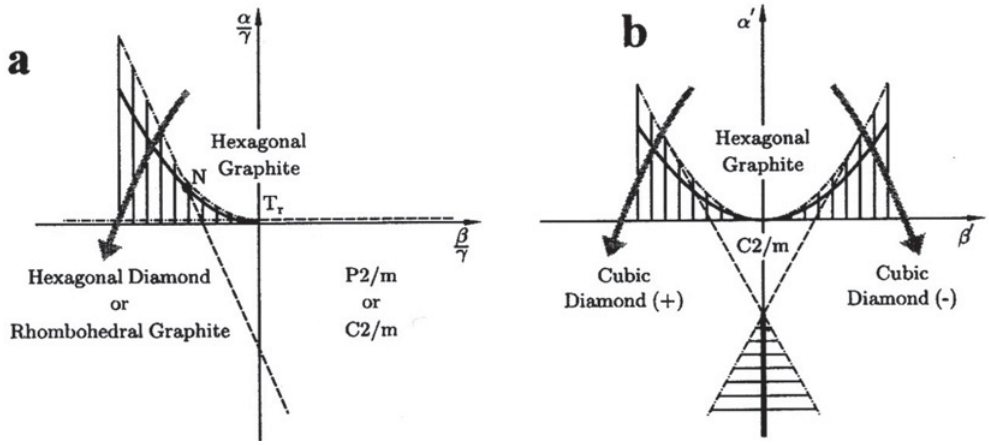

Figure 34. Theoretical phase diagrams corresponding to the minimization of the (**a**) $F_1(\eta(\xi))$ and (**b**) $F_2(\eta(\xi))$ Landau expansions, given in the text, with respect to the displacements ξ. Solid, dashed and dashed-dotted lines represent, respectively, first-order transition, second-order transition and limit of stability lines. The hatched areas are regions of phase coexistence. N is a three-phase point. T_r is a tricritical point. The arrows suggest the thermodynamic path followed in carbon.

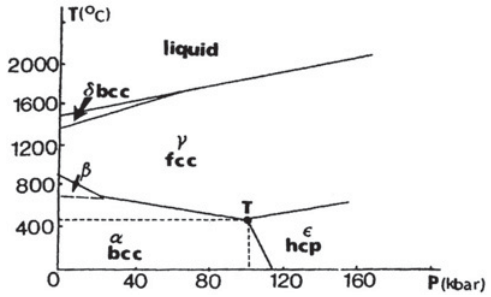

Figure 35. Schematic representation of the pressure-temperature phase-diagram of iron.

HD) transitions, and $F_2(\eta(\xi)) = \frac{\alpha'}{2}\eta^2 + \frac{\beta'}{3}\eta^3 + \frac{\gamma'}{4}\eta^4$, for the HG $\rightarrow$ CD transition. The corresponding theoretical phase diagrams are shown in Fig. 34. The left- or right-hand side of the theoretical phase diagram of Fig. 34(b), which exhibits only the HG and CD phases, reflects the topology of the experimental phase diagram of carbon [47]. The anti-isostructural CD variant may coincide with the cubic n-diamond structure [48], which is composed of hexagonal-ring planes puckered in the opposite direction with respect to CD.

6.4 The phase diagram of iron

Two of the most commonly encountered reconstructive mechanisms are found in the phase diagram of iron: the bcc $\rightarrow$ hcp Burgers mechanism [49], and the bcc $\rightarrow$ fcc Bain deformation mechanism [50]. The three α-bcc, γ-fcc and ε-hcp phases merge at a triple point and are separated by transition curves which are almost straight lines. The temperature-pressure phase diagram of iron, shown in Fig. 35, contains an additional δ-bcc phase in the low pressure-high temperature region below the melt, as well as a more recently discovered high-pressure β-phase, for which two different structures have been proposed: a double-hcp structure and an orthorhombic structure of symmetry *Pbcm* [51, 52]. The reconstructive mechanisms relating the different phases are shown in Fig. 36. They can be

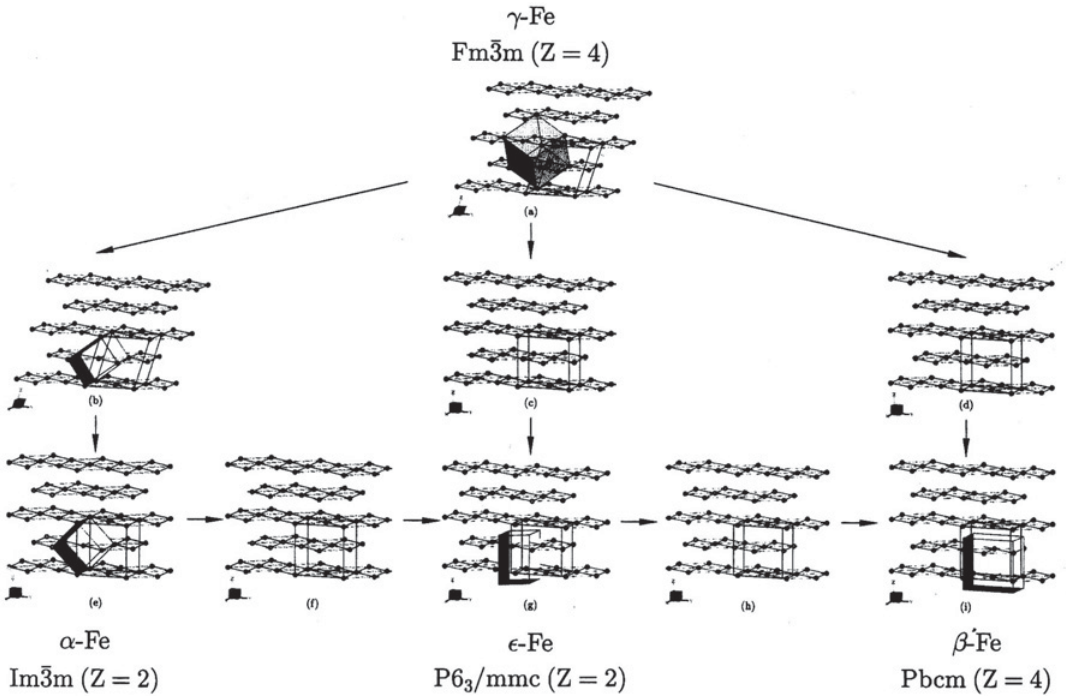

Figure 36. Structural mechanisms associated with the reconstructive transitions between the fcc γ-phase of iron and bcc $\alpha-$Fe or hcp $\varepsilon-$Fe. The intermediate substructure common to the three phases, represented in all the figures, has the symmetry $I4/mmm$ (Z = 1) for the $\gamma \rightarrow \alpha$ transition, and $Cmcm$ ($Z = 2$) for the $\gamma \rightarrow \varepsilon$ transition. The (a)$\rightarrow$(d)$\rightarrow$(i) path represents the reconstructive mechanism from $\gamma-$Fe to an eventual high-pressure β modification [52], the existence of which remains to be confirmed.

described as occurring via a common substructure having the monoclinic symmetry $C2/m$ (Z = 4). All the mechanisms can be expressed in terms of critical strains and fractional displacements [53]. The corresponding order-parameters are periodic functions of the critical displacements as represented in Fig. 37.

7. INCOMMENSURATE STRUCTURES AND THE CRYSTAL-AMORPHOUS TRANSITION

7.1 Landau theory of incommensurate structures

In the Landau theory the increment of the probability density describing the change in the spatial distribution of atoms in a crystal undergoing a phase transition reads:

$$\delta\rho^k = \sum_{i=1}^{p} \eta_i^k(\vec{r})\Psi_i^k(\vec{r}) \tag{44}$$

where the $\Psi_i^k(\vec{r})$ are normalized functions transforming as the basis of an irreducible representation of the parent space-group G_0, the $\vec{k}$-vector corresponding to a point of the Brillouin zone of the parent structure. The stable states of the crystal are characterized by definite values η_i^k of the order-parameter components associated with an absolute minimum of the transition free-energy $\Phi(\eta_i^k)$, expressed as a polynomial expansion of the η_i^k. Lifshitz has noted that when the transition leads to an inhomogeneous low-symmetry structure, the preceding condition does not test completely the stability of the phases

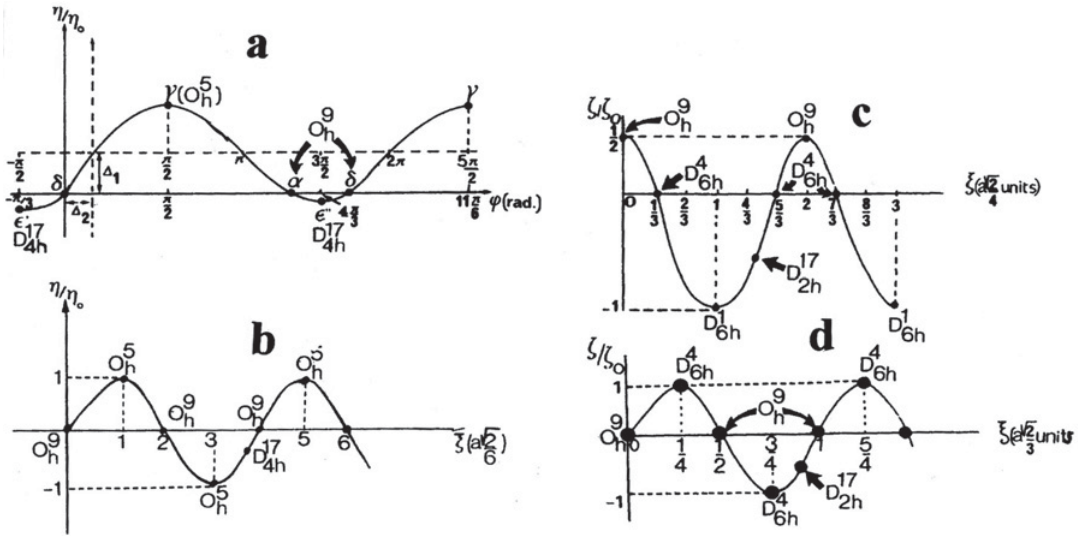

Figure 37. **(a)** and **(b)**: Periodic dependence of the order-parameter for the $\delta \rightarrow \gamma \rightarrow \alpha$ phase sequence in function **(a)** of the angle φ between the diagonals in the (110) cubic plane, and **(b)** of the displacements ξ along the [011] cubic direction. **(c)** and **(d)**: Periodic dependence of the order-parameter at the $\alpha \rightarrow \varepsilon$ transition in function of the displacements ξ along the $[1\bar{1}0]$ bcc direction. In **(d)** the geometrical constraints imposed by the size of the atoms is also taken into account.

at the macroscopic level, as $\Phi(\eta_i^k)$ has also to be minimum with respect to variations of the η_i^k, which vary continuously from one point to another in the low symmetry phase. As a consequence, instead of a homogeneous polynomial expansion for the free-energy, one has to consider a functional

$$\Phi(\eta_i^k, \frac{\partial \eta_i^k}{\partial x_j}) = \int \phi(\eta_i^k(\vec{r}))d\vec{r} \tag{45}$$

where the sum runs over the volume of the system, the free-energy density ϕ depending on the η_i^k and on their spatial derivatives. If the η_i^k vary slowly at the microscopic level, Lifshitz shows [54] that to determine the eventual stability of an inhomogeneous structure, it is sufficient to consider antisymmetric gradient invariants of the form $\eta_i^k \frac{\partial \eta_j^k}{\partial x_l} - \eta_j^k \frac{\partial \eta_i^k}{\partial x_l}$ with $i \neq j, (x_l = x, y, z)$. If such terms (called Lifshitz invariants) are allowed by the parent symmetry, an inhomogeneous phase may stabilize across a second-order transition from the parent phase. These ideas were used by Dzialoshinskii [55] in the description of incommensurate helimagnetic structures. In incommensurate structures the transition wave-vector varies with temperature (or pressure, or concentration) within an interval $\Delta\vec{k}$, and therefore one has to consider the variation of $\delta\rho^k(\vec{r})$ in this interval. Dzialoshinskii proposed to fix the value $\vec{k} = \vec{k}_c$, where $\vec{k}_c$ represents a rational vector associated with the lock-in transition, which generally takes place below the range of stability of the incommensurate phase. The physical assumption underlying this choice is that, within the incommensurate phase, the system is asymptotically governed by a periodic potential possessing the symmetry of the lock-in phase, i.e., the incommensurate structure is treated as a spatial modulation of the lock-in structure. As a consequence the Ψ_i^k functions form the basis of a single irreducible representation associated with $\vec{k}_c$, but the order-parameter components $\eta_i^{k_c}$ appear as slowly modulated functions of the actual order-parameter components η_i^k. As a consequence Φ is a continuous function of $\vec{k}$ through the sequence of parent-incommensurate-lock-in phases.

7.2 Phenomenological theory of the amorphous solid state

7.2.1 Basic assumptions of the model: The gauge invariant free-energy

An amorphous solid phase can be obtained by overcooling a liquid [56], by irradiating a crystal with different types of particles [57], or by pressurizing a crystal phase [58]. Although the microscopic mechanism and transformation kinetics depend on the amorphization process and class of materials, all amorphous phases show no long-range order and physical properties (solidity, high viscosity, small diffusion) which make the amorphous state essentially different from the liquid state [56]. An amorphous phase can be assumed to result from a parent crystal phase. This assumption is obviously justified for irradiation-induced and pressure-induced amorphizations. For glasses formed from a liquid one can consider as the parent phase the crystal phase bypassed on overcooling, since the local glass structure reflects the chemical bonding of the bypassed crystal. For introducing the model [59], let us assume that the order-parameter of the crystal amorphous transition has two complex components $\eta = \rho e^{i\varphi}$ and $\eta* = \rho e^{-i\varphi}$, where ρ and φ depend on the space coordinates $x_j (j = 1, 2, 3)$. At variance with the approach to incommensurate structures, *the critical wave vector* $\vec{k}$ *associated with the crystal-amorphous transition is assumed to vary continuously from one point to another of the amorphous phase*:

$$\vec{k}_c(x_j) = \sum_{k=1}^{3} \mu_k(x_j)\vec{t}_k^* \tag{46}$$

where the $\vec{t}_k^*$ are the reciprocal lattice vectors of the parent crystal phase, the μ_k coefficients varying continuously in space. This is consistent with assumed geometrical topology of amorphous structures in which each two neighbouring cells display different basic translations.

The primitive translation operators $\hat{t}_i$ of the parent crystal phase transform the order-parameter as: $\hat{t}_i\eta = e^{i\vec{k}.\hat{t}_{ic}}\eta$ and $\hat{t}_i\eta* = e^{-i\vec{k}_c.\vec{t}_i}\eta*$. Since $\vec{k}_c.\vec{t}_i = 2\pi\mu_i$, one has:

$$\hat{t}_i\eta = e^{2i\pi\mu_i}\eta \text{ and } \hat{t}_i\eta* = e^{-2i\pi\mu_i}\eta* \tag{47}$$

showing that η and $\eta*$ are eigen functions of $\vec{t}_i$ and form a continuous spectrum, the free-energy density ϕ of the crystal-amorphous transition containing the invariants $\eta\eta*$, $(\eta\eta*)^2$. By contrast one has:

$$\hat{t}_i\left(\frac{\partial\eta}{\partial x_j}\right) = e^{2i\pi\mu_i}\left(\frac{\partial}{\partial x_j} + 2i\pi\frac{\partial\mu_i}{\partial x_j}\right)\eta \tag{48}$$

expressing that the order-parameter derivatives *are not* eigen functions of $\hat{t}_i$. However, one can use *covariant derivatives,* which are invariant under $\hat{t}_i$. One can take here:

$$D_i\eta = \left(\frac{\partial}{\partial x_i} - i\gamma\sum_j A_{ji}\right)\eta \text{ and } D_i^*\eta* = \left(\frac{\partial}{\partial x_i} + i\gamma\sum_j A_{ji}\right)\eta* \tag{49}$$

where γ is a coupling constant, and the A_{ji} are components of a second-rank tensor transforming as:

$$\hat{t}_i(A_{ik}) = A_{ik} + 2\pi\frac{\partial\mu_i}{\partial x_k} \text{ and } \hat{t}_i A_{lk} = A_{lk}(l \neq k) \tag{50}$$

The physical meaning of the space-dependent (A_{ji}) tensor can be anticipated as representing a compensating *stress-field potential*, i.e., a gauge-field potential which ensures the local invariance under translation of the order-parameter derivatives. One has:

$$\hat{t}_i D_i\eta = e^{2i\pi\mu_i} D_i\eta \text{ and } \hat{t}_i^* D_i^*\eta* = e^{-2i\mu_i} D_i^*\eta* \tag{51}$$

Thus, the invariants $D_i\eta D_i^*\eta*, \eta D_i^*\eta*, \eta* D_i\eta$ can be included into the free-energy density ϕ, which is gauge invariant under the phase change $\eta \to \eta e^{2i\pi\mu_i}$. From Eq. (50) one finds the quadratic sums

$\sum_k \sigma_{ik}^2$ to be also gauge invariant, where:

$$\sigma_{ik} = \sum_{j,l} \varepsilon_{kjl} \frac{\partial A_{il}}{\partial x_k} \tag{52}$$

are *internal stress-field components*, and ε_{kjl} is the Levi-Civita tensor. Therefore the free-energy associated with he crystal-to-amorphous transition has the form: $\Phi = \int \phi \left(\eta, \eta*, D_i\eta, D_i^*\eta*, \frac{\partial A_{il}}{\partial x_k}\right) dV$ and can be minimized independently with respect to $\eta, \eta*$ and A_{ji}. For the purpose of our demonstration we take:

$$\phi = \frac{a}{2}\eta\eta* + \frac{b}{4}(\eta\eta*)^2 + \frac{c}{2}\sum_i D_i\eta D_i^*\eta* + \frac{d}{2}\sum_k \sigma_{ik}^2 \tag{53}$$

where a, b, c and d are phenomenological coefficients.

7.2.2 Analogy with Ginzburg-Landau theory of superconductivity

We now refer to the formal analogy existing between the equations describing the deformed states of a solid and Maxwell's equations of magnetostatics [60]. In this analogy the internal stress-field potential (A_{ji}) coincides with the vector potential $\vec{A}$, and the internal stress-field with the magnetic induction $\vec{B}$, Eq. (52) corresponding to $\vec{B} = curl\,\vec{A}$. It leads to another analogy between: 1) Our description of the amorphous state resulting from the breaking of the translational symmetry of the parent crystal phase, where the spatial dependence of the order-parameter gradient is compensated by a stress-field potential, and 2) the Ginzburg-Landau time independent description of the superconducting state [5], in which the gauge symmetry of the normal state is broken, and the spatial dependence of the gradient of the wave function $\Psi = |\Psi|e^{i\psi}$ is compensated by the vector potential $\vec{A}$. Substituting in Eq. (53) η by Ψ, $D_i\eta$ by $(\vec{\nabla} - \frac{4i\pi}{he}\vec{A})$, and σ_{ik} by $\vec{B}$, one gets the free-energy density used in the Ginzburg-Landau model [5]. Accordingly, minimization of Φ should yield equations, which are analogue to the Ginzburg-Landau equations, and constitute the equations of state of an amorphous solid. Minimizing Φ with respect to A_{ji} gives the analogue of $\vec{j} = curl\,\vec{H}$, relating the current density to the magnetic field. It reads:

$$\alpha_{ij} = \sum_{kl} \varepsilon_{jkl} \frac{\partial \omega_{il}}{\partial x_k} \tag{54}$$

which is Kröner equation [60] relating the *dislocation density tensor* $\alpha_{ij} = \frac{\partial \phi}{\partial A_{ij}}$ to the *distortion tensor* $\omega_{ij} = \frac{\partial \phi}{\partial \sigma_{ij}}$, the conservation of the dislocation current $\sum_j \frac{\partial \alpha_{ij}}{\partial x_j} = 0$ corresponding to div $\vec{j} = 0$. The α_{ij} components depend on the transition order-parameter and stress-field potential as:

$$\alpha_{ij} = -\gamma \frac{c}{d}\rho^2 \left(\frac{\partial \varphi}{\partial x_i} + \sum_j \gamma A_{ji}\right) \tag{55}$$

Minimization of Φ with respect to η and $\eta*$ gives

$$-c\left(\frac{\partial}{\partial x_i} + i\gamma \sum_j A_{ji}\right)^2 \eta + a\eta + b\rho^2\eta = 0 \tag{56}$$

and a similar equation of state for $\eta*$. Equations (54) to (56) show that the local state of an amorphous solid phase is stabilized by a stress-field deriving from a stress-field potential coupled to the crystal-amorphous order-parameter, which compensates the structural distortions and creates a stationary dislocation flux. In the absence of an internal stress-field the amorphous is unstable. This is in contrast to the property of the superconducting state to be stable in the absence of an applied magnetic field,

corresponding to a homogeneous state with constant amplitude and phase of the superconducting order-parameter. Therefore the amorphous state appears as the analogue of *the mixed state of type II superconductors* [61], the amorphous analogue of the Meissner effect consisting of a partial extrusion of the internal stress-field which lowers the local distortion and preserves a finite density of dislocations. Within this interpretation the homogeneous state with constant ρ and φ is a *superhard crystal phase* from which the stress-field is extruded, i.e., its structure remains undeformed under applied stress except close to its surface. One can show that:

$$\sigma_{ij}(x) = \sigma_{ij}^{0} \exp\left(-\frac{x}{\delta}\right) \tag{57}$$

where $\delta = \left(-\frac{bd^2}{\gamma^2 ac}\right)^{1/2}$ represents the *penetration length* of the stress-field inside the superhard crystal in the direction normal to the surface of the sample. Assuming $a = a_0(\varsigma_S - \varsigma)$ $(a_0 > 0)$, where ς is an applied stress (or pressure), and ς_S the critical stress at which the amorphous-to-superhard crystal transition takes place, Eq. (57) shows that with increasing applied stress $\varsigma > \varsigma_S$ the internal stress-field decreases exponentially, i. e. the penetration depth is limited to a near surface layer of thickness $\delta(\varsigma)$. Introducing the correlation length of the order-parameter fluctuations $\xi(\varsigma) = \left(-\frac{c}{2a}\right)^{1/2}$, the amorphous analogue of the Ginzburg-Landau parameter is $\chi = \frac{\delta(\varsigma)}{\xi(\varsigma)} = \left(2\frac{bd^2}{\gamma^2 c^2}\right)^{1/2}$, which for a type II superconductor fulfils the condition $\chi > 1/\sqrt{2}$. It yields the relationship between ς_S and the critical stress ς_A at which the amorphous state occurs:

$$\varsigma_S = \sqrt{2}\chi\varsigma_A = 2\left(\frac{bd^2}{\gamma^2 c^2}\right)^{1/2}\varsigma_A \tag{58}$$

where the condition $\frac{bd^2}{\gamma^2 c^2} > \frac{1}{4}$ is required for the amorphous phase to be stable.

Recrystallization of amorphous phases under pressure has been observed in amorphous $\alpha-$ quartz [62], which transforms into stishovite at about 60 GPa, and for the high-density amorphous phase of ice [63], which recovers the ice VII or ice VIII structure at high pressure. Recrystallization under pressure or stress is also observed in a number of glasses [64]. On the other hand, superhard properties, i.e. extremely low compressibility of the same order of magnitude as in diamond, have been reported for cubic boron nitride [65], the tridymite-like phase of carbon dioxide [66], or superhard graphite [67].

The most typical effect characterizing the mixed state of type II superconductors is the existence of vortices oriented in the direction of the applied magnetic field [61]. Their amorphous elastic analogs should be formed by defect lines, about which the wave-vector $\vec{k}_c(x_i)$ turns continuously due to the non-quantization of the stress-flux. At variance with superconducting vortices, amorphous elastic vortices are non-directional due to the tensorial character of the stress-field, and to the property of the applied and internal stresses to have different proper systems of coordinates. The defect lines can be formed, for example, by Somigliana-type dislocations [68], as suggested for glassy polymers [69], or by screw dislocations with variable Burgers vectors [70].

8. CONCLUSION

In this article the flexibility of the Landau theory for investigating different fields of condensed matter physics has been illustrated. The initial Landau approach, restricted to continuous phase transitions between strictly periodic structures, induced by a single irreducible representation of the parent space-group, has been shown to adapt to the description of first-order transitions, eventually associated with several order-parameters, or leading to incommensurate or amorphous phases, and to reconstructive transitions for which the symmetry relationship between the phases is apparently lost. Each extention requires some modification of the initial Landau model, but preserves the basic concepts of the model, i.e. the order-parameter and Landau expansion concepts. Symmetry and related group-theoretical considerations, as well as thermodynamics form the essential ingredients of the Landau

phenomenological approach, which constitutes and invaluable tool for understanding the physics of complex systems.

References

[1] L. D. Landau, Zh. Eksp. Teor. Fiziki 7, 19 (1937) and 7, 627 (1937). Translated in *Collected Papers of L. D. Landau*, Ed. D Ter Haar (Pergamon, Oxford, 1965), p. 193 and 216.
[2] J. C. Tolédano and P. Tolédano, *The Landau Theory of Phase Transitions* (World Scientific, Singapore, 1987), Chap. IV, and Ref. 3, Chap. I.
[3] P. Tolédano and V. Dmitriev, *Reconstructive Phase Transitions* (World Scientific, Singapore, 1996)
[4] Refs. 2, Chapters III and VI
[5] L. D. Landau and V. L. Ginzburg, Sov. Phys. JETP 20, 1064 (1950)
[6] L. D. Landau, Sov. Phys. JETP 11, 592 (1941)
[7] S. Alexander and J. Mctague, Phys. Rev. Lett. 41, 702 (1978)
[8] P. Tolédano, B. Mettout, M. Aroyo and J. M. Perez Mato, Phys. Rev. Lett. 95, 205701 (2005)
[9] P. G. de Gennes *The Physics of Liquid Crystals* (Clarendon, Oxford, 1974), and Ref. 2 Chap. VII.
[10] P. Tolédano and B. Mettout, in *Phase Transitions in Complex Fluids* (World Scientific, Singapore, 1998), Eds. P. Tolédano and A. M. Figueiredo Neto, p. 111
[11] P. Ehrenfest, Leiden Comm. Suppl. 675, 628 (1933)
[12] E. I. Kut'in, V. L. Lorman and S. V. Pavlov, Sov. Phys. Usp. 34, 497 (1991)
[13] Landöld-Börstein, *Ferro-and Antiferroelectric Substances,* (Springer-Verlag, Berlin, 1969), Band 3
[14] J. Holakovsky, Phys. Stat. Sol. (b) 56, 615 (1973)
[15] E. M. Lifshitz, Zh. Eksp. Teor. Fiziki 14, 353 (1944)
[16] K. Taniguchi et al., Phys. Rev. Lett. 97, 097203 (2006)
[17] G. Lautenschläger et al., Phys. Rev. B 48, 6087 (1993)
[18] E. P. Wigner, *Group Theory and its application to the quantum mechanics of atomic spectra* (Academic Press, New York, 1959)
[19] O. V. Kovalev, *The Irreducible Representations of space Groups* (Gordon and Breach, New York, 1965)
[20] V. Dvorak, V. Janovec and Y. Ishibashi, J. Phys. Soc. Jpn. 52, 2053 (1983)
[21] G. Lautenschläger et al., Phys. Rev. B 48, 6087 (1993)
[22] H. Sagayama et al, Phys. Rev. B 77, 220407 (2008)
[23] K. Taniguchi et al., Phys. Rev. Lett. 101, 207205 (2008)
[24] I. E. Dzialoshinskii, Sov. Phys. JETP 5, 1259 (1957)
[25] T. Moriya, Phys. Rev. 120, 91 (1960)
[26] H. Katsura, N. Nagaosa and V. Balatsky, Phys. Rev. Lett. 95, 057205 (2005)
[27] T. Kimura et al. Nature 426, 55 (2003)
[28] M. Kenzelmann et al., Phys. Rev. Lett. 95, 087206 (2005)
[29] P. Tolédano, Phys. Rev. B 79, 094416 (2009)
[30] H. Barath et al, Phys. Rev. B 78, 134407 (2008)
[31] J. Strempfer et al., Phys. Rev. B 75, 212402 (2007)
[32] P. Tolédano, W. Schranz and G. Krexner, Phys. Rev. B 79, 144103 (2009)
[33] N. Hur et al., Nature, 429, 392 (2004)
[34] L. C. Chapon et al., Phys. Rev. Lett. 93, 177402 (2004)
[35] Y. Noda et al., J. Phys. Condens. Matter, 20, 434206 (2008)
[36] L. C. Chapon et al., Phys. Rev. Lett. 96, 097601 (2006)
[37] N. Hur et al., Phys. Rev. Lett., 93, 107207 (2004)
[38] B. Mettout, P. Tolédano and V. Lorman, Phys. Rev. Lett. 77, 2284 (1996)

[39] P. Tolédano and A. M. Figueiredo Neto, Phys. Rev. Lett. 79, 4405 (1997)
[40] P. Tolédano and A. M. Figueiredo Neto, Phys. Rev. Lett. 84, 5540 (2000)
[41] V. P. Dmitriev, S. B. Rochal, Yu. M. Gufan and P. Tolédano, Phys. Rev. Lett. 60, 1958 (1988)
[42] O. Blaschko, V. P. Dmitriev, G. Krexner and P. Tolédano, Phys. Rev. B 59, 9095 (1999)
[43] V. P. Dmitriev, S. B. Rochal and P. Tolédano, Phys. Rev. Lett. 71, 553 (1993)
[44] P. Tolédano, Z. Kristallogr. 220, 672 (2005)
[45] H. Katzke, U. Bismayer and P. Tolédano, J. Phys. Condens. Matter 18, 5219 (2006)
[46] V. P. Dmitriev, S.B. Rochal, Yu. M. Gufan and P. Tolédano, Phys. Rev. Lett. 62, 2495 (1989)
[47] D. A. Young, *Phase diagrams of the Elements* (Berkeley, CA: University of California Press, 1991)
[48] H. Hirai and K Kondo, Science 253, 772 (1991)
[49] W. G. Burgers, Physica 1, 561 (1934)
[50] E. C. Bain, Trans. AIME 70, 25 (1924)
[51] S. Saxena, L. S. Dubrovinsky and P. Haggvist, Geophys. Res. Lett. 23, 2441 (1996)
[52] D. Andrault et al., Science, 278, 831 (1997)
[53] H. Katzke, D. Machon and P. Tolédano, unpublished
[54] E. M. Lifshitz, Zh. Eksp. Teor. Fiziki, 11, 255 (1941)
[55] I. E. Dzialoshinskii, Sov. Phys. JETP 19, 960 (1964)
[56] R. Zallen, *The Physics of amorphous solids* (Wiley, New York, 1983)
[57] S. Siegel, Phys. Rev. 75, 1823 (1949)
[58] O. Mishima, L. Calvert and E. Whalley, Nature 310, 393 (1984)
[59] P. Tolédano, Europhys. Lett. 78, 46003 (2007)
[60] E. Kröner, *Kontinumstheorie der Versetzungen und Eigenspannungen* (Springer, Berlin, 1958)
[61] A. A. Abrikosov, Sov. Phys. JETP 5, 1174 (1957)
[62] Y. Tsuchida and T. Yagi, Nature 347, 267 (1990)
[63] R. J. Hemley, L.C. Chen and H. K. Mao, Nature 338, 638 (1989)
[64] J. Z. Jiang et al., J. Mater. Res. 18, 895 (2003)
[65] E. Knittle et al., Nature 337, 349 (1989)
[66] C. S. Yoo et al., Phys. Rev. Lett. 83, 5527 (1999)
[67] W. L. Mao et al., Science 302, 425 (2003)
[68] J. C. M. Li, Metall. Trans. 16 A, 2227 (1985)
[69] C. G'Sell, Mater. Sci. Eng. A309-310, 539 (2001)
[70] P. Chaudhari, A. Levi and P. Steinhardt, Phys. Rev. Lett. 43, 1517 (1979)